

Future hotspots of compound dry and hot summers emerge in European agricultural areas

Andrea Boehnisch¹, Elizaveta Felsche¹, Magdalena Mittermeier¹, Benjamin Poschlod², and Ralf Ludwig³

¹Ludwig-Maximilians-Universität München

²Universität Hamburg

³Ludwig Maximilians Universität

September 11, 2023

Abstract

Compound dry and hot extremes (CDHE, such as recent summers 2015, 2018 and 2022 in Europe) have wide ranging impacts: Heat exacerbates moisture shortages during dry periods whereas water demand rises. Climate change will likely increase the intensity, frequency, and duration of CDHE events in Europe. However, current studies focus on drivers and impacts in coarse-resolution global climate models and likely miss spatial details of CDHE characteristics. To overcome this issue, we exploit a regional 50-member single-model initial condition large ensemble (SMILE) at 12 km spatial resolution. Hence 1000 model years per 20 year-periods provide an extensive database of CDHE and robust estimations of their occurrence changes across Europe in high geographical detail. CDHE occurrences are investigated in a current climate and at two global warming levels (+2 °C, +3 °C). We identify Northern France, Southern Germany, Switzerland, Southern Ireland, and the western coasts of the Black Sea with currently low CDHE frequencies as emerging hotspots. These regions experience a tenfold occurrence increase under global warming conditions. Apart from Western Europe, temperature is the dominant contributor to frequency increases. Furthermore, tail dependencies strengthen in regions with high CDHE frequency increases. In European agricultural areas, soil moisture shows very strong negative correlations with CDHE extremeness. Last, our results suggest a halving of CDHE in a +2 °C world compared to a +3 °C world, highlighting the necessity of climate mitigation with respect to this hazard type.

1 **Future hotspots of compound dry and hot summers**
2 **emerge in European agricultural areas**

3 **Andrea Böhnisch¹, Elizaveta Felsche^{1,2}, Magdalena Mittermeier¹, Benjamin**
4 **Poschlod³, Ralf Ludwig¹**

5 ¹Department of Geography, Ludwig-Maximilians-Universität München, Munich, Germany

6 ²Center for Digital Technology and Management, Munich, Germany

7 ³Research Unit Sustainability and Climate Risk, Center for Earth System Research and Sustainability,
8 Universität Hamburg, Hamburg, Germany

9 **Key Points:**

- 10 • During compound dry and hot extreme (CDHE) summers, latent heat flux is markedly
11 reduced in widespread areas of the European continent.
- 12 • The frequency increase of CDHE events, associated with extremely low soil mois-
13 ture, doubles under GWL3 compared to GWL2.
- 14 • CDHE frequency increases are predominantly driven by rising temperature, with
15 regional contributions of bivariate tail dependence increases.

Corresponding author: Andrea Böhnisch, a.boehnisch@lmu.de

Abstract

Compound dry and hot extremes (CDHE, such as recent summers 2015, 2018 and 2022 in Europe) have wide ranging impacts: Heat exacerbates moisture shortages during dry periods whereas water demand rises. Climate change will likely increase the intensity, frequency, and duration of CDHE events in Europe. However, current studies focus on drivers and impacts in coarse-resolution global climate models and likely miss spatial details of CDHE characteristics. To overcome this issue, we exploit a regional 50-member single-model initial condition large ensemble (SMILE) at 12 km spatial resolution. Hence 1000 model years per 20 year-periods provide an extensive database of CDHE and robust estimations of their occurrence changes across Europe in high geographical detail. CDHE occurrences are investigated in a current climate and at two global warming levels (+2 °C, +3 °C). We identify Northern France, Southern Germany, Switzerland, Southern Ireland, and the western coasts of the Black Sea with currently low CDHE frequencies as emerging hotspots. These regions experience a tenfold occurrence increase under global warming conditions. Apart from Western Europe, temperature is the dominant contributor to frequency increases. Furthermore, tail dependencies strengthen in regions with high CDHE frequency increases. In European agricultural areas, soil moisture shows very strong negative correlations with CDHE extremeness. Last, our results suggest a halving of CDHE in a +2 °C world compared to a +3 °C world, highlighting the necessity of climate mitigation with respect to this hazard type.

Plain Language Summary

During the last years, summers tended to be exceptionally dry and hot at the same time. Dry and hot conditions affect various economic and ecologic sectors, for example agriculture by soil moisture reduction. Assessing their frequency and intensity under climate change conditions is hence pivotal to develop effective adaptation strategies. The particularity of this study is a so-called regional climate model large ensemble: Its 50 simulations from the same model are equally probable realizations of climate trajectories. We thus investigate 1000 model years for a current climate, a +2°C and +3°C warmer world at high geographical detail. This allows for robust analysis as numerous events occur per period. We show that hot and dry summers become more frequent, mostly because of warming with some regions affected by both warming and drying. Furthermore, we find a strengthening link between high temperature and low precipitation, which is often not considered in studies. Additionally, lower soil moisture conditions in agricultural areas coincide with more extreme dry and hot summers. In a +3°C world, these events are projected to occur at least twice as frequent as in a +2°C world. This stresses the relevance of climate change mitigation efforts.

1 Introduction

Triggered by an accumulation of recent events, the temporal co-occurrence of extremely dry and hot conditions has sparked a large literature body. Globally, but especially in Europe, simultaneous droughts and heatwaves rank first among multivariate hazard investigations (Afroz et al., 2023). Up to 20 % of heatwaves coincided with droughts since the 1980s (rising trend; Mukherjee & Mishra, 2021). In Europe, droughts during the warm season – often accompanied by heatwaves – increasingly emerge as the dominant drought type (Markonis et al., 2021). For instance, the year 2018 exhibited unprecedented dry and hot conditions during spring to summer in the northern hemisphere (Buras et al., 2020). Vegetation, thriving from suitable growing conditions in spring, aggravated soil depletion by summer due to enhanced transpiration (Bastos et al., 2020).

Heatwaves and droughts share common drivers, albeit on different effective time scales (Miralles et al., 2019). This is reflected in the general negative correlation of temperature and precipitation (Zscheischler & Fischer, 2020; Trenberth & Shea, 2005). For

66 example, in 2018 anticyclonic blocking through April–October over central Europe, in
67 particular a stationary pattern that was recurrently associated with heat anomalies over
68 Europe and North America, favored persistent dry and hot conditions (Buras et al., 2020;
69 Toreti et al., 2019; Rousi et al., 2023; Kornhuber et al., 2019). Buras et al. (2020) also
70 show the close spatial correspondence of high pressure, hot extremes (which typically oc-
71 cur below anticyclonic conditions, Kornhuber et al., 2019), and water budget deficits.
72 This context can be explained by drying and warming in descending air masses, which
73 exacerbate atmospheric evaporative demand such that subsequently increased evapotran-
74 spiration may reduce soil moisture (e.g., Zscheischler et al., 2020). Dry soils in turn heat
75 up more quickly and thus support the sensible heat flux (e.g., Schwingshackl et al., 2017).
76 The warming effect in humid areas during hot and dry conditions due to enhanced net
77 radiation is dampened by evaporative cooling, which is induced by vegetation transpi-
78 ration and soil evaporation (O et al., 2022). In arid areas, generally low soil water con-
79 tents and dry vegetation constrain latent heat and amplify temperature increases via en-
80 hanced sensible heat fluxes (O et al., 2022). Locally, drought conditions precede extreme
81 heat in summers (Felsche et al., 2023), while simultaneous drought conditions may pro-
82 long heatwaves via land-atmospheric coupling (Fischer et al., 2007).

83 This relationship is mutual: Manning et al. (2019) suggest that enduring and in-
84 tense hot and dry conditions also trigger soil moisture droughts, and Mukherjee et al.
85 (2023) find amplifying soil effects in both drought–heat and heat–drought cascades. In
86 Germany, soil moisture depletion and precipitation deficits during summer 2018 resulted
87 in a shift from commonly energy-limited to moisture-limited evaporative regimes (Rousi
88 et al., 2023). Soil moisture deficits, however, considerably hamper vegetation produc-
89 tivity (Bastos et al., 2020). In summer 2018, the general water budget was more strongly
90 affected in European agricultural and pasture regions than in forests, but vegetation de-
91 graded in both arable and forest regions (Buras et al., 2020). Crop yields of major plants
92 in Northern and central Europe were halved compared to the preceding 5 years (Toreti
93 et al., 2019). In the similarly hot and dry summer of 2003, European gross and net pri-
94 mary production decreased by up to 30 % and 20 %, respectively (Ciais et al., 2005). While
95 heat was shown to mostly affect crop yields, droughts additionally kill the plants (Lesk
96 et al., 2016). Thus a co-occurrence of both extremes also bears the potential to merge
97 impacts, especially by affecting soil moisture as a pre-condition for crop development.

98 The impacts of compounding extremes are hence amplified compared to its single
99 components. This holds also true for compound dry and hot extreme (CDHE) events,
100 as mentioned previously. Literature describes various kinds of compound events, e.g., pre-
101 conditioned, temporally or spatially compounding, and multivariate types (e.g., Zscheis-
102 chler et al., 2020). CDHE can be considered as multivariate, in that two hazards co-occur
103 simultaneously in time and space due to their common drivers, or as pre-conditioned if,
104 e.g., soil moisture conditions of previous seasons were taken into account (Zscheischler
105 et al., 2020). Identifying compound events with joint distributions, in this case of tem-
106 perature and precipitation, allows their investigation via multivariate probability distri-
107 bution functions, i.e., copulas (Bevacqua et al., 2017; Zscheischler et al., 2020). These
108 represent dependencies among the variables and can be used to derive multivariate ex-
109 treme value probabilities (Zscheischler et al., 2020). Event occurrence probabilities in
110 turn can be expressed as return periods. For instance, return periods for the CDHE grow-
111 ing season 2018 exceed several thousand years for certain event definitions (Zscheischler
112 & Fischer, 2020). Especially in situations where adaptation and decision making rely on
113 return periods, such as water resources management, bivariate analyses are essential. With-
114 out considering the bivariate dependence structure, there is a risk of both overestimating
115 or underestimating the occurrence of events (Bevacqua et al., 2017): For instance,
116 bivariate return periods of the 2014 California winter drought, one of the first CDHE to
117 be investigated bivariately, were shown to be higher than univariate precipitation deficit
118 return periods owing to extremely high winter temperatures (AghaKouchak et al., 2014).

Most studies on bivariate events focus on prominent cases without gaining generalized knowledge on the event–impact relationships by, e.g., aligning event extremeness with impact extremeness. Examples for this approach include the calculation of (standardized) temperature and precipitation ratios or products (Hao et al., 2018; Mukherjee & Mishra, 2021), but without considering the variable dependencies. Others employ water budget deficits as CDHE intensity surrogate (Buras et al., 2020). In this study, we consider bivariate return periods as an intensity surrogate. Since they indicate the joint extremeness of the considered variables, higher return periods also correspond to higher temperatures and lower precipitation in the CDHE case. To illustrate the intensity of the bivariate return periods, we align soil moisture to the CDHE.

In order to evaluate low-frequency compound events and derive meaningful knowledge on their effects on soil moisture, observational records provide too few events. Hence, ensembles of climate model simulations are beneficial to enlarge the event sample. However, for the investigation of compound events, it is advisable to be sure about comparable process representation in all used simulations (e.g., regarding the joint temperature–precipitation distribution). Both issues can be addressed by accessing single-model initial condition large ensembles (SMILEs) (e.g., Maher et al., 2021). SMILEs consist of several simulations of the same model under the same external forcing conditions (i.e., scenario), differing only due to their initial conditions. Global SMILEs proved to be a skillful tool for the reduction of uncertainty due to internal variability in multivariate event attribution (Bevacqua et al., 2023). However, it is a known issue that compound events require finer spatial resolution if realistic information for adaptation planning on a regional scale is sought (François & Vrac, 2023).

The goal of this study is thus to (a) obtain and explain spatially explicit frequency changes in European CDHE summers (June–August, JJA) under three global warming levels and (b) relate the ranked events with soil moisture as a relevant condition for impacts on agriculture. In order to reduce sampling uncertainties from a statistical perspective and address internal climate variability, we employ a regional high resolution SMILE.

2 Materials and Methods

2.1 Regional Large Ensemble Data for robust sampling

Investigating low-probability compound events of extremes requires an abundant data base. We therefore employ the regional SMILE of the Canadian Regional Climate Model, version 5 (CRCM5-LE; Leduc et al., 2019). The CRCM5-LE was developed within the ClimEx project: 50 members of the Canadian Earth System Model, version 2, Large Ensemble (CanESM2-LE; Fyfe et al., 2017; Kirchmeier-Young et al., 2017) were dynamically downscaled with the CRCM5 to obtain 50 high-resolution (0.11° , corresponding to 12.5 km) time series of 1950–2099 over two domains, Europe and Northeastern North America (Leduc et al., 2019). The original members of the CanESM2-LE were constructed by applying small random perturbations to the long-term control run in 1850 and subsequently in 1950. After a few years, the 50 members are considered to be independent due to the chaotic nature of weather sequences, while still following the same forcing conditions (RCP8.5 from 2006 onward) and thus pertaining comparable climate statistics (Leduc et al., 2019).

The CRCM5-LE already proved its value for compound analyses of hydro-meteorological extremes, namely rain on saturated soil and rain-on-snow events (Poschod et al., 2020). Further, this regional SMILE was used for investigation of heatwaves (Böhnisch et al., 2023), droughts (Böhnisch et al., 2021), and heat and drought linkage at an inter-seasonal scale (Felsche et al., 2023).

2.2 Global Warming Levels in a regional climate model

We employed global warming levels (GWL) for our analysis of future climate projections. This approach has been widely applied because it has the advantage of being less sensitive to the selected model and scenario. Furthermore, it allows to directly compare the warming rate to the goal of the Paris Agreement of limiting global warming to “(...) well below 2 °C above pre-industrial levels and to pursue efforts to limit the temperature increase to 1.5 °C (...)” (UNFCCC, 2015). The GWLs were calculated as anomalies in the yearly global mean surface air temperature (*tas*) to the pre-industrial reference period 1850–1900 (Hauser et al., 2022; Seneviratne et al., 2021). GWLs refer to a 20-year period centered around the first year, in which the warming level is exceeded ($tas > GWL$). The methodology is based on Hauser et al. (2022), which was used for the Sixth Assessment Report of the Intergovernmental Panel on Climate Change (IPCC). We adopted the code for the use in the CanESM2-LE. To this end, we pooled all 50 members before calculating the anomalies to 1850–1900.

Our reference period 2001–2020 translates to $GWL = +1.2$ °C (GWL1.2) in CanESM2-LE (observed approximately 1 °C; Gulev et al., 2021). This is less an effect of the forcing scenario for RCP8.5 was shown to be in high agreement with observed emissions (Schwalm et al., 2020). Instead, it mirrors the model’s rather high equilibrium climate sensitivity (3.7 K; Swart et al., 2019). Comparing modeled global *tas* with observational global mean temperature though may result in an overestimation partly due to insufficient observational data coverage and blending air temperature over land with sea surface temperatures over ocean areas in observations (Richardson et al., 2016; Vogel et al., 2019).

Future periods in our study are represented by 20-year slices centered at $GWL = +2$ °C (GWL2, Paris Agreement; UNFCCC, 2015) and $GWL = +3$ °C (GWL3, close to the most realistic end-of-century temperature of 2.8 °C under current trends in climate policy; Liu & Raftery, 2021).

Time periods corresponding to a given GWL were calculated within the global SMILE, and adopted for use in the regional SMILE.

2.3 Definition and Bivariate Evaluation of Compound Events

2.3.1 Event Definition

This study takes a multivariate perspective on dry and hot extremes, since we are particularly interested in the combined occurrences of these hazards. We employed thus the “AND” hazard scenario to connect both univariate extremes (Zscheischler & Fischer, 2020): the temporal co-occurrence of linearly detrended summer mean temperatures and (negative) precipitation sums exceeding the respective 95th percentile of 2001–2020 (with the 95th percentile of negative precipitation equaling the 5th percentile; see Supplementary figure S1). By definition, these events are expected to be very rare because both variables have to exceed a high threshold. However, since JJA temperature and negative precipitation show strong correlations in most parts of Europe, which intensified during the 21st century, CDHE occur more often than would be implied by independence (Zscheischler & Seneviratne, 2017). This implies that warm summers are commonly dry and wet summers are cool (see also Trenberth & Shea, 2005; Wang et al., 2021). Due to the extensive large ensemble database, 1000 years instead of 20 years (see fig. 1 (a)) are available per analysis period and allow for robust baseline definition (i.e., percentile estimates across all 50 ensemble members) and event characteristic estimation (e.g., frequency changes, associated behavior).

In order to characterize CDHE summer energy partitioning compared to non-CDHE summers, we employed the Bowen Ratio (BR, Bowen, 1926). The BR describes the ratio of sensible heat flux and latent heat flux, which are negatively coupled (e.g., Schwing-

shackl et al., 2017). For this analysis, we used the model variables surface upward latent heat flux and surface upward sensible heat flux.

2.3.2 Estimation of Bivariate Return Periods

In order to estimate the joint extremeness of CDHEs, we calculated bivariate return periods. Generally, return periods are the inverse of the (annual) exceedance probability p of a given event intensity, the return level z_p . Hence, the return level z_p is expected to be exceeded every $1/p$ years, defining thus the return period $T = 1/p$ (Coles, 2001). Bivariate return periods however remain ambiguous and become larger than their univariate component return periods due to the second variable that is required to meet the extremes condition as well (AghaKouchak et al., 2014; Zscheischler & Fischer, 2020). In large samples like the CRCM5-LE, (annual) event occurrences per time period can be counted and inverted to obtain the return period (Zscheischler & Fischer, 2020). This empirical approach is generally limited by the time series length. With 1000 years available, 10 events with $T = 100$ are to be expected statistically, while the most extreme case would be $T = 1000$. Any inference on this level would be highly uncertain since it is based on a single event (e.g., Zscheischler & Fischer, 2020). For shorter time series, the maximum empirical T also decreases such that extreme event estimation suffers from high uncertainties (Bevacqua et al., 2017). Instead of event counting, we here fitted copulas, i.e., multivariate probability distributions, to the bivariate distributions (Zscheischler & Fischer, 2020). The large advantage of distribution fitting is the option for pushing the rareness boundaries of the empirical approach.

For the procedure in this study we used the R package *VineCopula* (Nagler et al., 2023). First, we transformed the empirical marginals of summer temperature and precipitation (multiplied with -1 for calculation purposes) to uniform distributions on $[0,1]$. Next, the most suitable copula family was estimated using the Bayesian Information Criterion (BIC) and fitted to the data. For this study, we chose the locally best fitting copula family from eight single-parametric copula families (fig. S3).

Following the relation in Brunner et al. (2016), the return period T was obtained by:

$$T(u, v) = \frac{\mu}{1 - u - v + C(u, v)} \quad (1)$$

giving the probability for jointly exceeding the event defining thresholds in the denominator, with u, v corresponding to univariate probabilities of exceeding the respective threshold, $C(u, v)$ being the copula at (u, v) , and the mean interarrival time $\mu = 1$ in our case since we investigated annual events (Zscheischler & Fischer, 2020; Zscheischler & Seneviratne, 2017; Brunner et al., 2016).

2.3.3 Distributional Change Assessments

Both changes in temperature and precipitation may lead to frequency changes by shifting the bivariate distribution compared to the reference period. Additionally, the bivariate (tail) dependence structure may change over time.

In order to address the first point, we here propose a method to disentangle the dominating drivers of frequency changes. Horizontal shifts of the distribution (along the orange line in fig. 1 (b)) indicate temperature changes as sole drivers whereas vertical shifts (along the blue line in fig. 1 (b)) point to precipitation changes. Any change with both a horizontal and vertical component thus is due to a combination of temperature and precipitation changes. For the definition of the dominating driver, we used the average JJA drying per degree warming (fig. 1 (b)): In Europe, the slope of this relation-

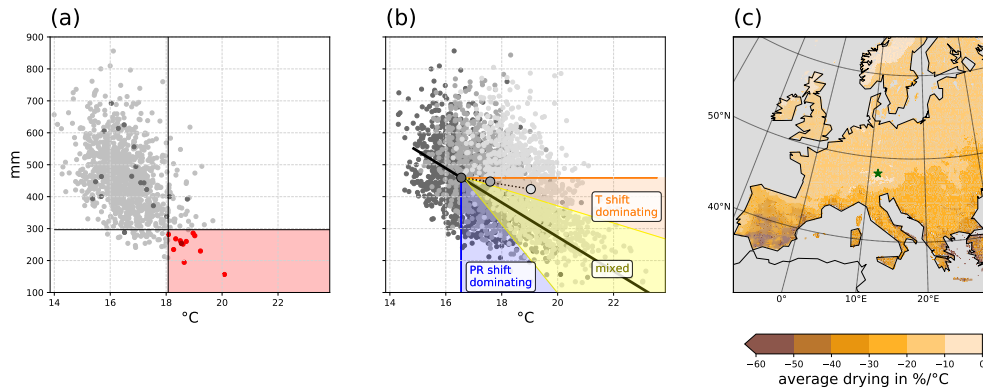


Figure 1. (a) Precipitation and temperature of 1000 summers (50 members for 2001–2020) over a grid cell representing Munich/Germany (star in (c)). Dark grey and dark red dots show the limited sample of one arbitrary member. Black lines indicate the 95th percentile of temperature (vertical) and 5th percentile of precipitation (i.e., the 95th percentile of negative precipitation; horizontal) with the red area highlighting all summers meeting the definition criterion for a CDHE. (b) Definition of temperature (orange) and precipitation (blue) dominance in distributional shifts under climate change conditions. Yellow indicates mixed contributions of temperature and precipitation (see text). Grey shaded point clouds correspond to current, GWL2, and GWL3 climates for the same pixel as in (a). The black line represents the local average summer drying scaled with warming. (c) Average summer drying scaled with warming expressed as slopes of a linear line fitted to the local bivariate distribution.

262 ship follows a North–South gradient with highest values in the Mediterranean area and
 263 especially over the Iberian Peninsula where summer precipitation is very low (fig. 1 (c)).
 264 Distributional shifts along this slope represent the occurrence of more extreme events
 265 by heating and drying following the current relationship. If the center of the distribu-
 266 tion is shifted within the orange sector of fig. 1 (b), temperature is identified as dom-
 267 inating driver, while it is precipitation for shifts into the blue sector. Since we are also
 268 interested in simultaneous changes of temperature and precipitation, we introduced a
 269 buffer zone between a line with half the local slope and a line with twice the local slope
 270 to account for uncertainties in slope estimation (yellow sector). This combination is fur-
 271 ther referred to as mixed drivers. This approach is based on correlation of the full dis-
 272 tributions, which, as Zscheischler and Seneviratne (2017) argue, can serve as an indica-
 273 tor for the likelihood of CDHE if the percentile threshold for event definition is not too
 274 high.

275 To account for dependencies in the distribution extremes, tail (= extremal) depen-
 276 dence above the 95th univariate percentiles ($\chi(0.95)$; Coles et al., 1999) were cal-
 277 culated for each period separately using the R package *extRemes* (Gilleland, 2022). Con-
 278 fidence intervals at the 0.05 level were obtained by bootstrapping 1000 times.

279 2.4 Assessment of CDHE Impacts on Soil Moisture

280 In one of the first compound event definitions by Leonard et al. (2014), compound
 281 events are defined by the extremeness of impacts originating from multiple contribut-
 282 ing hazards. While our CDHE definition rather follows a hazard-based perspective, we
 283 nevertheless aim to assess CDHE effects in this study. Our (univariate) target variable
 284 is soil moisture, classified as the soil moisture index (SMI) of Zink et al. (2016), which
 285 also forms the basis of the German Drought Monitor. The SMI is based on soil mois-

286 ture percentiles of a reference period (2001–2020 in our case). We used JJA soil mois-
 287 ture in the upper portion of the soil column to assess agricultural droughts during cur-
 288 rent climate, GWL2, and GWL3. Soil moisture is especially useful when assessing event
 289 impacts, for soil moisture droughts have large agricultural and ecosystem-specific impacts.
 290 Assessing soil moisture conditions is hence most relevant in areas where they potentially
 291 have an impact. Therefore, we confined our analyses of CDHE–soil moisture relation-
 292 ships on European agricultural areas. These comprise Corine Land Cover (CLC2018 ver-
 293 sion 2020_20u1, linearly regridded to CRCM5-LE spatial resolution; EEA, 2020) level-
 294 2 classes *arable land*, *permanent crops*, and *heterogeneous agricultural areas*.

295 3 Results

296 3.1 Bowen Ratio Increases During CDHE

297 CDHE and non-CDHE summers differ with respect to the energy-partitioning of
 298 sensible and latent heat flux. In order to illustrate these differences in a spatially explicit
 299 way, we first look at the Bowen Ratio during summer under current climate conditions.
 300 During non-CDHE summers, the latent heat flux, i.e., evaporative cooling (O et al., 2022),
 301 is dominating over the sensible heat flux in large areas of Europe (fig. 2 (a)–(b)). These
 302 coincide with the wet evapotranspiration regions (energy-limited) of Schwingshackl et
 303 al. (2017). The dominating low BR conditions favor widespread cloud formation and sum-
 304 mer precipitation. In CDHE summers (fig. 2 (b)), however, BR increases in large areas.
 305 High BR occurs in their wet/transition regions (moisture-limited). Zscheischler et al. (2015)
 306 state that under dry conditions, evapotranspiration and temperature are strongly dom-
 307 inated by soil moisture. Especially the Mediterranean regions, the lower course of the
 308 Danube and coastal regions of the Black Sea experience $BR > 10$. Under these condi-
 309 tions, a reduced latent heat flux (and hence evaporation) suggests low soil moisture avail-
 310 ability, while temperatures rise (Mukherjee et al., 2023). Consequently, cloud convec-
 311 tion and precipitation are inhibited.

312 We find no BR inversions or only small increases during CDHE in Northern and
 313 central Europe as well as in mountainous regions (fig. 2 (a)–(b)). However, these regions
 314 are characterized by evaporation increases (and hence soil drying) during CDHE sum-
 315 mers (fig. 2 (c)). This suggests an increase in latent heat flux and, potentially, a reduced
 316 temperature increase due to evaporative cooling (O et al., 2022). These regions are char-
 317 acterized by an energy-limited evapotranspiration regime (Teuling et al., 2009), where
 318 higher temperatures in CDHE summers compared to non-CDHE summers favor evap-
 319 oration. The remainder of the domain, largely defined by soil-moisture limited evapo-
 320 transpiration regimes (Teuling et al., 2009), experiences major evaporation reductions
 321 (fig. 2 (c)), presumably due to moisture limitations in comparison to non-CDHE sum-
 322 mers. High BR values, i.e., low latent heat flux compared to sensible heat flux, may re-
 323 sult from low soil moisture conditions (Trenberth & Shea, 2005). Since soil moisture and
 324 evaporation mutually influence each other and CDHE affect evaporation (Miralles et al.,
 325 2019), we conclude here that soil moisture is affected by CDHE occurrences as well.

326 The described relationships for CDHE and non-CDHE hold true for GWL2 and
 327 GWL3 (see supplementary fig. S2 for BR evolution under GWL2 and GWL3).

328 3.2 CDHE Frequency Increases

329 CDHE occur rarely under current climate conditions (fig. 3 (a)). Assuming no de-
 330 pendence between temperature and precipitation, the occurrence probability of a CDHE
 331 would amount to $0.05 \times 0.05 = 0.0025 = 0.25$ events per 100 years. This corresponds
 332 to a 1-in-400 year event. This very rare frequency is however exceeded over most of Eu-
 333 rope. Assuming total dependence, the frequency has an upper limit at 5 events per 100
 334 years by definition of the CDHE events, equaling a 1-in-20 year event. In the CRCM5-

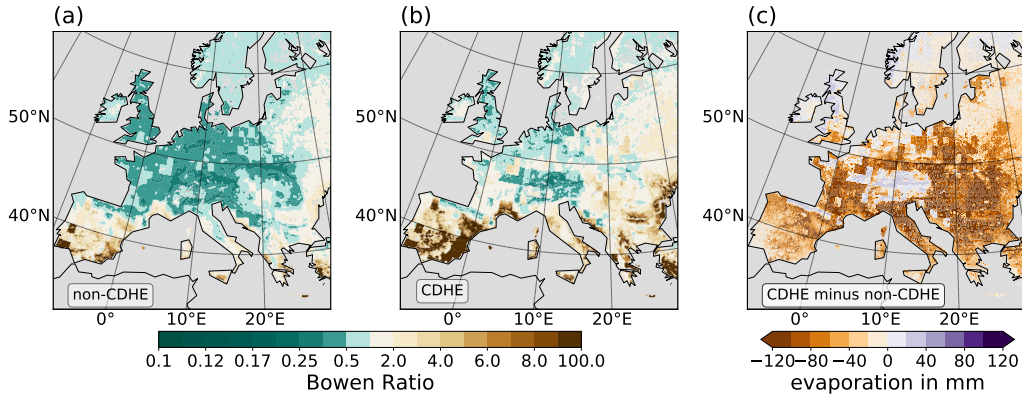


Figure 2. Bowen Ratio for non-CDHE summers (a) and CDHE summers (b) under current climate conditions. The median across all ensemble members is shown per category. Brownish colors indicate regions with sensible heat $>$ latent heat, greenish colors indicate regions with sensible heat $<$ latent heat. (c) evaporation increases (purple) and decreases (orange) in CDHE summers compared to non-CDHE summers under current conditions.

335 LE, highest event frequencies reach 3.5 events per 100 years in central eastern Europe
 336 (roughly 1-in-28 year event). On the contrary, parts of the Mediterranean, Aegean and
 337 Black Sea coastal regions as well as Southern Ireland, Northern France, and mountain-
 338 ous regions in central and Northern Europe encounter $<$ 0.5 events per 100 years which
 339 corresponds to a 1-in-200 year event.

340 For GWL2, event frequencies regionally double to triple, with strongest increases
 341 in Southern Europe and weakest changes in Northern and central eastern Europe as well
 342 as the Western Iberian Peninsula (fig. 3 (b)). No decreases are detected. Interestingly,
 343 while some regions with highest event frequencies under current conditions, e.g., central
 344 eastern Europe, encounter only increases by $<$ 3 events per 100 years, Southeastern France
 345 both shows high frequencies under current conditions and strong increases under GWL2.
 346 Contrasting to that, the coastal areas of the Mediterranean, Aegean and Black Sea with
 347 low event occurrences under current conditions experience an even higher increase by
 348 6–9 events per 100 years.

349 With further ascending GWL, event frequencies surge (fig. 3 (c)): Especially in moun-
 350 tainous forelands of Northern/Northeastern Spain and central/Southwestern France more
 351 than 1 out of 4 years under GWL3 qualify as a CDHE with respect to current percentile
 352 definitions (adding frequencies in fig. 3 (a) and (c)). The same holds true for the Po Val-
 353 ley in Northern Italy. Regions north of the Alps, in Northern France, Southern Ireland
 354 or the Western Iberian Peninsula with currently very few events ($<$ 0.5 per 100 years)
 355 experience up to $>$ 15 events per 100 years in addition to current frequencies. East-
 356 ern Europe and the Balkans are characterized by a North–South gradient of increases.
 357 Lowest gains are found in Scandinavia, Northeastern Europe, the highest Alpine ridges,
 358 and Southern Spain. To put these numbers into perspective, Toreti et al. (2019) show
 359 that 2018-like droughts mirror typical summer conditions by the 2040s, using a multi-
 360 model ensemble under RCP8.5.

361 3.3 Drivers of CDHE Frequency Increases

362 What is driving these frequency increases? In fig. 4, we investigate changes in the
 363 bivariate distribution of temperature and precipitation. First, fig. 4 (a)–(b) demonstrate
 364 the prevalent dominance of temperature increases in shifting the distribution into the

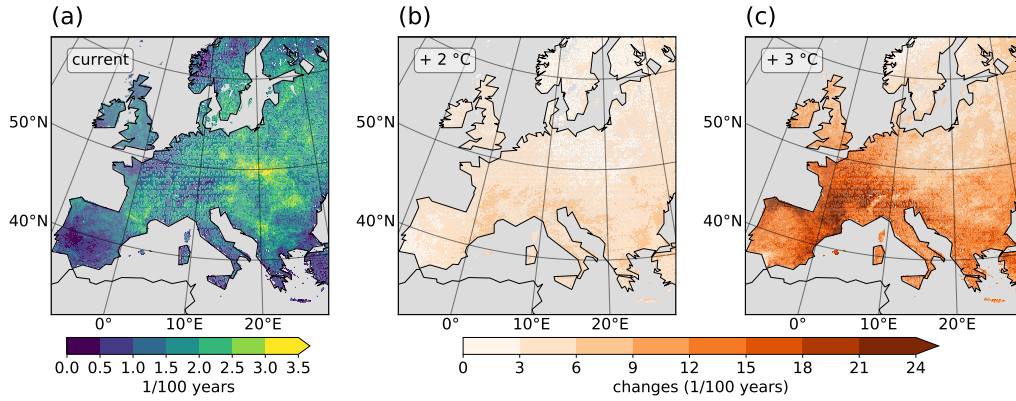


Figure 3. CDHE frequency for three global warming levels (absolute values for present climate (a) and changes under GWL2 (b) and GWL3 (c)). Events are defined as local exceedance of the current (2001–2020) 95th percentile of temperature and (negative) precipitation.

365 defined CDHE diagram space (see also fig. 1 (b)) under both GWL2 and GWL3. Pre-
 366 cipitation dominates in mountainous Norway and Northern Spain. In the Atlantic re-
 367 gions of Western Europe, temperature and precipitation changes jointly foster frequency
 368 increases. Under GWL3 conditions, these areas with mixed drivers expand towards the
 369 East. In addition, precipitation dominance emerges from previously mixed driver regions.
 370 This finding mirrors earlier emergence of (mean summer) temperature trends compared
 371 to higher uncertainty and variability in precipitation trends (e.g., von Trentini et al., 2019;
 372 Seneviratne et al., 2021). For large parts of Europe, precipitation variability defines hence
 373 whether a CDHE occurs, if (nearly) every year exceeds the present temperature thresh-
 374 old of event definition (consistent with e.g., Zscheischler & Fischer, 2020).

375 Secondly, we consider the dependence structure of the distributions (fig. 4 (c)–(e)).
 376 As stated above, a tail dependence of 1 implies that each temperature extreme (as de-
 377 fined here) is associated with a precipitation extreme and vice versa. The joint occur-
 378 rence probability of CDHE is thus 0.05 (i.e., 5 events per 100 years) and hence the same
 379 as for univariate extremes in our definition. On the contrary, a tail dependence of 0 im-
 380 plies independent behavior of temperature and precipitation extremes and thus a prob-
 381 ability of $0.05 \times 0.05 = 0.0025$ (i.e., 0.25 events per 100 years in our case). It follows
 382 that the spatial distribution in fig. 4 (c) mirrors the spatially distributed CDHE frequen-
 383 cies (fig. 3 (a)) with highest tail dependence corresponding to highest event frequencies
 384 in central eastern Europe and bivariate tail independence in mountainous Norway, North-
 385 ern France, Southern Ireland, inner Alpine regions, and Mediterranean coastal regions
 386 with very rare CDHE occurrence. Under GWL2, the tail dependence exceeds the cur-
 387 rent 95 % confidence interval especially in regions with currently low tail dependence val-
 388 ues (e.g., Northeastern France and Northern Italy, the Danube delta or mountainous Nor-
 389 way, fig. 4 (d)). In these regions, the tail dependence increase may add to event frequency.
 390 Tail dependence reductions are found on the western Iberian Peninsula with already low
 391 values and, notably, in central eastern Europe with currently highest values. More spa-
 392 tially distinct clusters emerge under GWL3 (fig. 4 (e)), where robust tail dependence in-
 393 creases occur in Northern France, Southern UK and Ireland, the Alpine (foreland) and
 394 Cantabrian Mountain regions, and Scandinavia. Tail dependence decreases, e.g., in South-
 395 ern Sweden, parts of the Iberian Peninsula, and central eastern Europe. In South-western
 396 Spain, this decrease may contribute to the rather low CDHE occurrence increase under
 397 GWL3 conditions (see fig. 3 (c)). Tail dependence changes are reflected by changes in
 398 the underlying copula family (supplementary fig. S3 (a)–(c)): For example, tail depen-

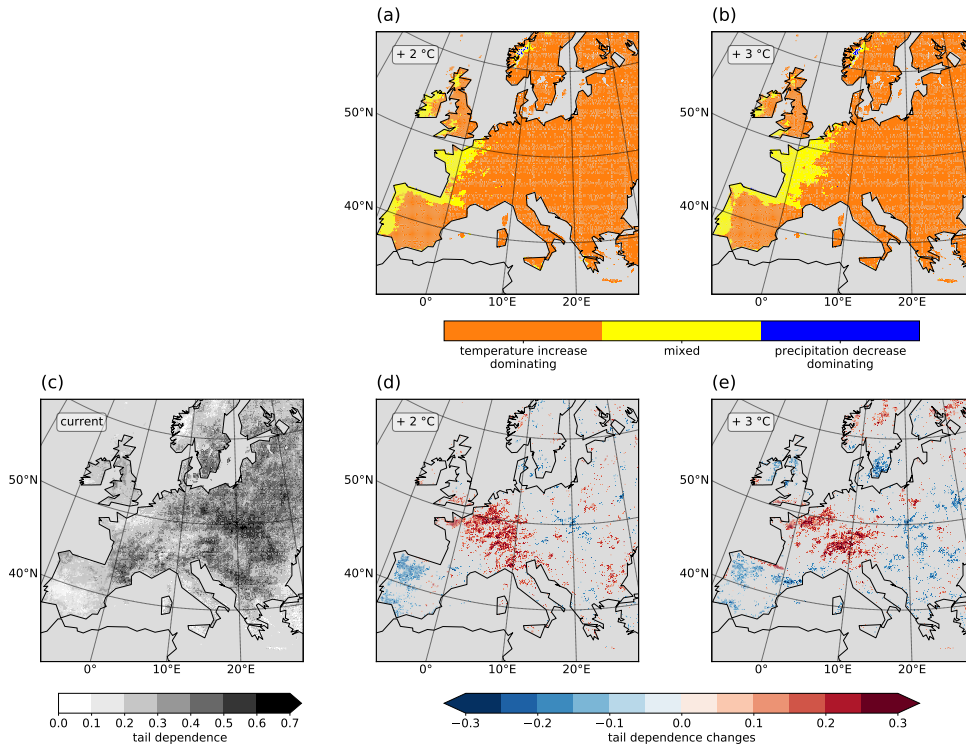


Figure 4. Changes in combined temperature and precipitation distributions. (a)–(b) distributional shifts due to temperature increases (orange), precipitation decreases (blue) or both (yellow) following the approach from fig. 1 (b)). Only land areas with significant correlations of JJA temperature and precipitation are colored. (c)–(e) tail dependence of temperature and (negative) precipitation: (c) current absolute values, changes for GWL2 (d) and GWL3 (e). For GWL2 and GWL3 only regions with changes exceeding the present 95 % confidence interval are shown. Note: The tail dependence refers to the tails above the respective 95th temperature and (negative) precipitation percentile of each period.

399 dence increases mostly correspond to switches from symmetric copula families (mostly
 400 Gaussian or Frank) to asymmetric families (e.g., Gumbel which only occur in regions with
 401 $BR < 1$ under current conditions). Decreases are associated with the inverted switch.
 402 Symmetric families represent regions with amplified tail dependence in the hot-dry and
 403 cold-wet tail, whereas asymmetric families include only one tail with enhanced depen-
 404 dence. Note that the bivariate structure is generally weak to moderate in most regions
 405 (theoretical Kendall's τ with $0.2 < \tau < 0.5$, fig. S2 (d)–(f)), pointing towards rather
 406 similar bivariate distributions. With increasing GWL, τ increases in Western Europe,
 407 hence strengthening the differences between the joint summer temperature–precipitation
 408 distributions.

409 The tail dependence also allows for a quick change of perspective: Since it is cal-
 410 culated with respect to each period (current, GWL2, GWL3), we are also able to infer
 411 that CDHEs defined relative to the percentiles of each period occur more (less) frequently
 412 where tail dependence increases (decreases).

413 3.4 Soil Moisture Scaling with CDHE Extremeness

414 To account for the risk that agricultural droughts, i.e., soil moisture deficits, pose
 415 on crops, we focus our further assessment on European agricultural regions.

416 We start our assessment with return periods T of CDHE in current, GWL2, and
 417 GWL3 conditions (fig. 5 (a)–(c)). Therefore, we ask the question: How extreme would
 418 a future CDHE be in relation to the current temperature and precipitation distribution?
 419 Since higher return periods correspond to hotter and drier summers with respect to cur-
 420 rent CDHE, they are interpreted as surrogates for joint event intensity. T is obtained
 421 for the 95th percentile of temperature and (negative) precipitation of the respective pe-
 422 riods from the copula fitted to the present bivariate distribution. Hence under current
 423 conditions (fig. 5 (a)), the distribution again mirrors the current tail dependence (fig. 4 (c))
 424 and event frequency distribution (fig. 3 (a)). The theoretical minimum return period of
 425 the current period is $T = 20$ (perfect tail dependence), the maximum $T = 400$ (inde-
 426 pendence). Consistent with that, we find among the CDHE just passing both thresh-
 427 olds return periods of $T = 30$ to $T = 300$ in the current period. Under GWL2 condi-
 428 tions (fig. 5 (b)), return periods increase to several hundreds to thousands of years with
 429 respect to the current distribution. In single grid cells (dark red), the extremeness of these
 430 CDHE is unprecedented ($T = \text{inf.}$). In these cases, (mostly) future temperature or pre-
 431 cipitation lie outside the margins of the current distribution. Hence CDHE of this ex-
 432 tremeness did not occur at all in the current period of the CRCM5-LE. Under GWL3
 433 (fig. 5 (c)), these CDHE are dominating across Europe: We find $T = 1000$ to $T = 3000$
 434 years in eastern Germany, Poland, and the Baltics, whereas the remainder of Europe is
 435 subject to CDHE with a current occurrence probability $p = 0$. To generalize, the con-
 436 ditions of CDHE definition correspond to highly unlikely current conditions when con-
 437 sidering GWL2, and unprecedented conditions in GWL3.

438 During all summers exceeding the respective CDHE definition in current, GWL2,
 439 and GWL3 climates (fig. 5 (d)–(f)), extreme (below 5th percentile) or exceptional droughts
 440 (below 2nd percentile) prevail in European agricultural regions. Exceptions are very southerly
 441 parts (Southern Spain, Turkey) where the soil moisture content corresponds to moder-
 442 ate (below 20th percentile) or severe (below 10th percentile) droughts. However, since
 443 SMI classes are calculated with respect to the local distribution and the local distribu-
 444 tions do not always range from total depletion to total saturation, the ‘less severe’ cat-
 445 egories may represent low absolute soil moisture conditions as well, while more severe
 446 drought conditions in humid regions may represent higher absolute soil moisture con-
 447 ditions. With rising GWL, virtually all European agricultural areas experience excep-
 448 tional drought conditions during future CDHE.

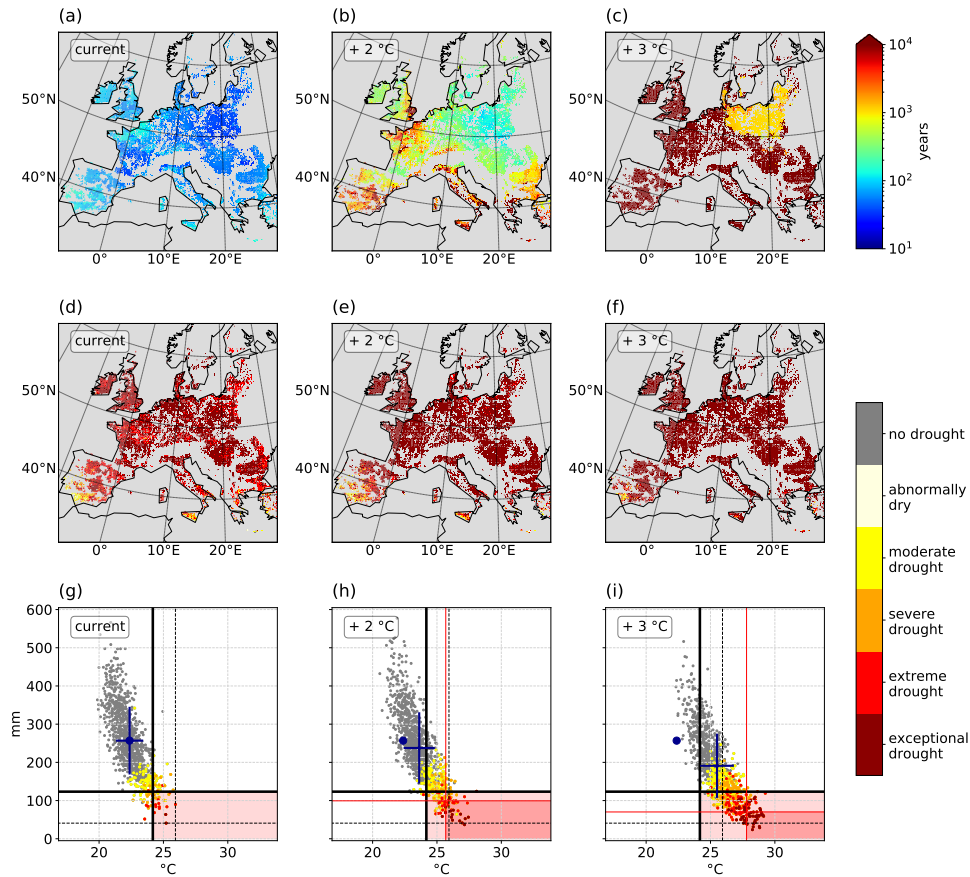


Figure 5. CDHE intensity for current, GWL2 and GWL3 conditions in European agricultural regions. (a)–(c) return period of summers with temperatures and (negative) precipitation at the GWL-specific 95th percentile (crosses of thick black lines in (g) and red lines in (h) and (i)). (d)–(f) average SMI categories during all summers exceeding the GWL-specific 95th percentiles of temperature and (negative) precipitation. (g)–(i) scatter plots of summer precipitation against summer temperature for an example region (Po Valley, Northern Italy). Thick (thin) black lines show the present 5th and 95th percentiles (minimum and maximum) for precipitation and temperature, respectively. Red lines mark the 5th and 95th percentiles for GWL2 and GWL3. Light red background highlights current CDHE summers; strong red background CDHE summers for GWL2 and GWL3 percentiles. Blue dots show the current mean, crosses span one standard deviation of the respective periods for temperature and precipitation. Colors in (d)–(i) indicate soil moisture drought categories (percentiles) with respect to the current period following Zink et al. (2016).

449 Figures 5 (g)–(i) further show the relationship among soil moisture droughts and
 450 compound events in an example region (Po Valley, south of the Alps) to illustrate the
 451 relationship between temperature, precipitation and SMI in all summers: Summers within
 452 the shaded diagram space (i.e., CDHE) are affected by more extreme SMI categories in
 453 all periods; under GWL3 the majority of CDHE summers corresponds to ‘exceptional
 454 drought’ (fig. 5 (i)). Soil moisture drought extremeness follows the distributional axis,
 455 (i.e., not dominantly along the temperature or precipitation axis). With progressing global
 456 climate change, distribution shifts towards warmer and drier conditions (see crosses re-
 457 lative to blue dots in (h) and (i)) increase the frequency of summers within the light red
 458 shaded diagram space and also more extreme SMI. The majority of CDHE summers in
 459 GWL2 and GWL3 is characterized by unprecedented temperatures (dotted black ver-
 460 tical line) and numerous future events undercut the driest current summer as well (dot-
 461 ted black horizontal line). This fact illustrates why this region is colored in dark red in
 462 fig. 5(c). CDHE frequencies even increase with respect to the future percentiles (dark
 463 red shaded diagram space) which aligns with risen tail dependence in this region (fig. 4 (h)–
 464 (i)). Overall, figs. 5 (g)–(i) suggest a stable relationship of high (low) absolute temper-
 465 ature (precipitation) values and soil moisture drought categories.

466 Last, how is bivariate extremeness of summers related to SMI? Figures 6 (a)–(c)
 467 provide Spearman rank correlations well below -0.8 in most of European agricultural ar-
 468 eas. This strong relationship implies that more extreme CDHE translate to lower mois-
 469 ture conditions. Note that the correlation does not allow to conclude whether CDHE are
 470 triggered or enhanced by low SMI values or vice versa, e.g., via land-atmosphere feed-
 471 backs. As discussed in Manning et al. (2019) and Mukherjee et al. (2023), both is plau-
 472 sible and most likely interconnected. In addition, soil moisture effects from previous sea-
 473 sons or years (Felsche et al., 2023; Bastos et al., 2020) may confound the effect of CDHE
 474 on soil moisture conditions of the same summer. The correlation is highly linear in all
 475 GWLs (fig. 6 (d)–(f)), with a shift from low event extremeness and high soil moisture
 476 in the example region during current conditions to high event extremeness and low soil
 477 moisture conditions under GWL3. Again, this mirrors large projected CDHE frequency
 478 increases both in absolute terms and relative to all summers of a given GWL epoch. These
 479 summers hence pose a triple hazard to ecosystems and agriculture in the affected regions,
 480 arising from low soil moisture, high temperature and thus high water demand for trans-
 481 piration, and low precipitation.

482 4 Discussion

483 In this study, we assessed frequency increases of European CDHE within a regional
 484 SMILE, drivers of these increases, and the association of CDHE with soil moisture droughts.
 485 The study does not provide insights in the causal directions of the SMI–CDHE relation-
 486 ship, i.e., answer the question whether low soil moisture results in or from CDHE occur-
 487 rence.

488 Defining CDHE based on summer precipitation percentiles comes at a cost as we
 489 found in our results: In very dry regions, precipitation fluctuates on a low level. Hence,
 490 due to the local JJA precipitation distribution, absolute differences between years be-
 491 low or above the percentile threshold are rather small. Here, temperature variability de-
 492 fines whether a CDHE occurs during a given period. Note that this is a different effect
 493 than precipitation variability driving CDHE occurrence in areas where regional warm-
 494 ing induces yearly exceedance of the temperature threshold. Compared to the remain-
 495 der of the domain, lag effects may play a more important role in soil moisture contents
 496 in areas with very low JJA precipitation sums. In general, CDHE may be more precisely
 497 defined with a Survival Kendall hazard definition instead of the AND definition (see, e.g.,
 498 in fig. 5 (g)–(i), Salvadori et al., 2016). However, the correlation of SMI and CDHE ex-
 499 tremeness is highly linear even in our simplified event definition.

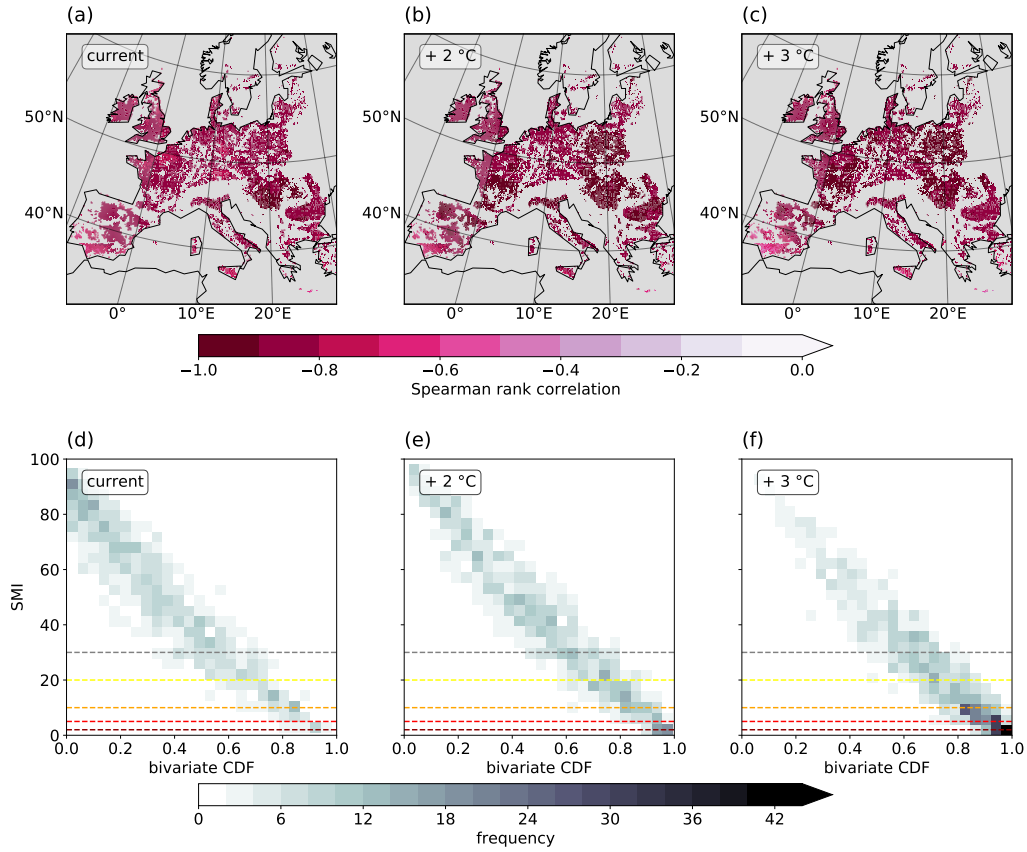


Figure 6. Relationship between CDHE extremeness (relative to conditions of the current period) and SMI values. (a)–(c) Spatially distributed Spearman rank correlation of CDHE extremeness and SMI values. (d)–(f) bivariate histograms of spatially aggregated CDHE extremeness and SMI in an example region (Po Valley, Northern Italy). Colors indicate the amount of summers in a given square. Dashed lines correspond to abnormally dry (grey), moderate drought (yellow), severe drought (orange), extreme drought (red), and exceptional drought (dark red) SMI conditions expressed as percentiles following Zink et al. (2016).

500 For explaining CDHE frequency increases, we focused on temperature and precip-
 501 itation mean shifts, i.e., no variability or higher-order distributional changes which are
 502 represented, e.g., in the marginal changes in François and Vrac (2023). Inspections of
 503 local distributions showed that for summer CDHE variability changes only marginally
 504 under GWL2 and GWL3 (e.g., fig. 5 (d)–(f)). Shifts of the joint distributions alone were
 505 shown to considerably increase CDHE frequencies – not only in arid regions as done by
 506 Hao et al. (2018) and Mukherjee and Mishra (2021), but also in transitional/humid re-
 507 gions. Our approach is limited by the margins of the current temperature and precip-
 508 itation distributions since we relate future events to the current distribution. Neverthe-
 509 less, we showed that the joint increase of hot and dry extremeness can be used as a qual-
 510 itative intensity measure. Beyond that, Wang et al. (2021) pointed to regionally inten-
 511 sifying negative correlations between temperature and precipitation over the last decades
 512 which led to an increase of CDHE, especially in the form of more heat events during droughts.
 513 However, we show that not only correlation of the full distribution is projected to change
 514 with rising GWL, but also the distributional tails and the entire dependence structure.
 515 Bivariate dependence structures in models though require cautious consideration. Zscheischler
 516 and Fischer (2020) point towards an underestimation of temperature and precipitation
 517 tail dependence in CMIP5 models. This would imply a potential underestimation of CDHE.
 518 A more detailed investigation into bivariate distributional characteristics in model and
 519 observational data is hence advisable for locally specific assessments.

520 By reaching GWL3 in the middle of the 21st century (2042–2061) under RCP8.5,
 521 the CanESM2 driving the CRCM5-LE proves to be a rather hot global climate model.
 522 We therefore used a relative model- and scenario-independent measure of time, i.e., the
 523 GWL, to overcome the effect of an intrinsically ‘hot’ global climate model with a high-
 524 emission scenario. Assessing uncertainties related to this approach requires comparative
 525 studies in other model SMILEs and with other scenarios. Yet, so far, there is only a very
 526 limited number of regional SMILEs (typically with only few members) available (e.g.,
 527 Aalbers et al., 2018).

528 As argued in Jha et al. (2023), the selection of warming levels and models explains
 529 most of the uncertainty in CDHE changes over Europe. The choice of copula families
 530 contributes the least in their assessment, while Zscheischler and Fischer (2020) argue that
 531 event definition and copula fitting affect the final probability and therefore extremeness
 532 of events. In our study, we attempted to reduce this kind of uncertainty by not focus-
 533 ing on single events. Instead, the SMILE served as a basis for investigating general char-
 534 acteristics of a large number of events, thus reducing the influence of outliers. Testing
 535 several copula families helped to find the locally best fitting bivariate distribution. Fur-
 536 ther, while in principle the SMILE provides the required size to sample low-probability
 537 events ($T = 1000$), we found that future events tend to be clearly more rare than cur-
 538 rent 1-in-1000 year events. Hence, even the large ensemble is insufficient for empirical
 539 estimations and distributional sampling is necessary.

540 Using the SMILE though allows for a robust sampling of internal variability which
 541 potentially masks dependence changes in setups with few members (Bevacqua et al., 2023).
 542 In addition, differing states of large-scale atmospheric modes prevalent in single mem-
 543 bers during the selected period of investigation may trigger differences in compound event
 544 frequencies (Bevacqua et al., 2023). This shows the high importance of internal variabil-
 545 ity in the evaluation of low-probability events and justifies the use of a SMILE.

546 While the CRCM5-LE provides high geographical detail in the spatial distribution
 547 of frequency (changes), results are affected by coarse resolution geophysical inputs as is
 548 visible in fig. 2: The tiling pattern resolution (1°) is coarser than the CRCM5 resolution,
 549 but finer than the spatial resolution of the driving general circulation model CanESM2.
 550 In central Europe, high bedrock depths (i.e., large soil column) coincide particularly well
 551 with low BR in fig. 2 (b) and high evaporation in fig. 2 (c). Presumably, a large soil col-
 552 umn contributes more strongly to evaporation than neighboring areas with thin soil columns.

553 However, this assumption requires further investigation, as well as implications on the
 554 reliability of other variables. For instance, this effect is also visible in the upper distri-
 555 butional tail of temperature at high temporal resolution (see also Miller et al., 2023). In
 556 spite of this, the regional SMILE allowed to highlight hotspots of event frequency (changes)
 557 and regionally varying driver dominance in high geographical detail. This is a large ad-
 558 vantage of our study over similar analyses with coarse-resolution global SMILEs: For ex-
 559 ample, a distinction of coastal or mountainous regions would not be possible on a coarse
 560 grid since the small-scale features cannot be resolved. Hence, the derivation of relevant
 561 drivers or dependence changes would have been impeded.

562 Given considerable frequency increases of CDHE and their association to low soil
 563 moisture contents, we argue that the relationship between both deserves further inves-
 564 tigation. Denissen et al. (2022) show that soil moisture limited conditions represent the
 565 new normal under a high-emission global warming scenario in that they intensify and
 566 expand in length. Since it has been shown that heatwaves, droughts or compound CDHE
 567 can be triggered by depleted soils (Fischer et al., 2007), investigating CDHE effects on
 568 soil moisture is also crucial in bringing forth the research on potential legacy effects on
 569 subsequent seasons or years (e.g., CDHE triggering subsequent CDHE mediated by pre-
 570 vailing soil depletion). CDHE may exert influence not only on temporally, but also spa-
 571 tially distant events: Li et al. (2023) show that dry soils in upwind regions may lead to
 572 propagation of events and, adding onto local land-atmosphere coupling, affect crop yields
 573 downwind of events. For example, these authors found that maize failure in Southeast-
 574 ern Europe and wheat failure in Italy tend to be associated with dry and hot conditions.

575 5 Conclusions

576 We find that European compound hot and dry summers are characterized by an
 577 increase of evaporative demand in the atmosphere, but with reduced evaporation in most
 578 regions, presumably due to soil moisture deficits. Mountainous regions experience increased
 579 evaporation, most likely due to higher temperatures and still dominant energy limita-
 580 tion of their evaporation regime. The frequency of CDHE summers increases consider-
 581 ably in Europe under climate change conditions. Owing to the high spatial resolution
 582 of our SMILE, we robustly identify regions in Southern France and Northern Spain as
 583 hotspots due to highest absolute increases, whereas, e.g., Southern Germany, Northern
 584 France, Southern Ireland, or the southwestern Black Sea coast can be identified as cur-
 585 rently low-frequency areas with highest multiplication of events under climate change.
 586 Apart from Western European regions, Northern Spain and mountainous Norway, fre-
 587 quency increases can be mostly attributed to rising temperatures. Yet, climate change
 588 also affects the bivariate dependence structure of temperature and precipitation, foster-
 589 ing tail dependencies and hence the co-occurrence of dry and hot conditions. Further,
 590 events intensify with respect to the current conditions of precipitation and temperature.
 591 Soil moisture during CDHE is projected to remain extremely low under GWL2 and GWL3
 592 in agricultural regions and shows particularly strong negative correlations with bivari-
 593 ate summer intensity.

594 This study finds newly emerging CDHE hotspots in European areas with yet un-
 595 seen combinations of extremely hot and dry conditions. Regardless of the causal direc-
 596 tions in the SMI-CDHE relationship, the tight relationship of low soil moisture and CDHE
 597 therefore poses an increasing risk to agriculture that requires consideration in adapta-
 598 tion planning.

599 This study also shows an ordering of temperature and precipitation changes in driv-
 600 ing the frequency increases: For GWL2, temperature increase is the major driver of CDHE
 601 frequency increases. For GWL3, precipitation decrease additionally emerge as impor-
 602 tant driver (in the form of mixed contributions). Here, it would be interesting to further
 603 investigate the processes and mechanisms driving local dependence increases or decreases.

604 The regional SMILE is particularly apt for analyzing compound events in the ex-
 605 tremite tails of the bivariate distribution. Climate change is shown to produce events that
 606 are much rarer than any observed summer, while currently extremely rare events become
 607 the new normal. Fitting distributions instead of counting the summers that meet the
 608 event definition criteria hence allows to avoid a saturation effect related to the maximum
 609 empirical event rareness under current conditions (i.e., $T = 1000$ years). Using SMILEs,
 610 further research can elucidate potential benefits of increasing sample sizes in reducing
 611 the uncertainty ranges of distribution fitting for extremely rare events.

612 Last, we conclude that limiting global warming to +2 °C considerably reduces CDHE
 613 hazards in Europe, which regionally then results in half the amount of summers with ex-
 614 tremely low soil moisture availability. Since the risk of impacts on human systems de-
 615 pends on resilience structures in the affected regions (e.g., Lesk et al., 2016), hazard re-
 616 duction should be accompanied by fostering resilience towards CDHE effects as well.

617 Open Research Section

618 The CRCM5-LE data used for all performed analyses is described in Leduc et al.
 619 (2019) and available at <https://www.climex-project.org/en/data-access/>

620 Corine land cover data is provided by the European Union, Copernicus Land Mon-
 621 itoring Service 2018, European Environment Agency (EEA) at [https://land.copernicus.eu/pan-](https://land.copernicus.eu/pan-european/corine-land-cover)
 622 [european/corine-land-cover](https://land.copernicus.eu/pan-european/corine-land-cover)

623 Codes to perform the presented analyses and obtain the figures will be shared through
 624 a public repository upon publication of the manuscript.

625 Acknowledgments

626 This research was conducted within the ClimEx project (www.climex-project.org) funded
 627 by the Bavarian State Ministry for the Environment and Consumer Protection (Grant
 628 No. 81-0270-024570/2015). CRCM5 was developed by the ESCER Centre of Université
 629 du Québec à Montréal (UQAM; <https://escer.uqam.ca/>, last access: 14 June 2023) in
 630 collaboration with Environment and Climate Change Canada. Computations with the
 631 CRCM5 for the ClimEx project were performed on the HPC system SuperMUC and the
 632 Linux Cluster of the Leibniz Supercomputing Center LRZ, Bavarian Academy of Sci-
 633 ences and the Humanities (BAdW), funded via GCS by BMBF and StMWFK. The au-
 634 thors gratefully acknowledge the Leibniz Supercomputing center for funding this project
 635 by providing computing time on its Linux-Cluster. Further, the authors would like to
 636 thank H. Funk for fruitful discussions on copula use.

637 References

- 638 Aalbers, E. E., Lenderink, G., van Meijgaard, E., & van den Hurk, B. J. J. M.
 639 (2018). Local-scale changes in mean and heavy precipitation in western eu-
 640 rope, climate change or internal variability? *Climate Dynamics*, *50*, 4745-
 641 4766. Retrieved from <https://doi.org/10.1007/s00382-017-3901-9> doi:
 642 10.1007/s00382-017-3901-9
- 643 Afroz, M., Chen, G., & Anandhi, A. (2023). Drought- and heatwave-associated com-
 644 pound extremes: A review of hotspots, variables, parameters, drivers, impacts,
 645 and analysis frameworks. *Frontiers in Earth Science*, *10*. Retrieved from
 646 <https://www.frontiersin.org/articles/10.3389/feart.2022.914437>
 647 doi: 10.3389/feart.2022.914437
- 648 AghaKouchak, A., Cheng, L., Mazdiyasni, O., & Farahmand, A. (2014). Global
 649 warming and changes in risk of concurrent climate extremes: Insights from
 650 the 2014 california drought. *Geophysical Research Letters*, *41*(24), 8847-8852.
 651 Retrieved from <https://agupubs.onlinelibrary.wiley.com/doi/abs/>

- 652 10.1002/2014GL062308 doi: <https://doi.org/10.1002/2014GL062308>
- 653 Bastos, A., Ciais, P., Friedlingstein, P., Sitch, S., Pongratz, J., Fan, L., ... Zaehle, S.
654 (2020). Direct and seasonal legacy effects of the 2018 heat wave and drought
655 on european ecosystem productivity. *Science Advances*, 6(24), eaba2724. Re-
656 trieved from <https://www.science.org/doi/abs/10.1126/sciadv.aba2724>
657 doi: 10.1126/sciadv.aba2724
- 658 Bevacqua, E., Maraun, D., Hobæk Haff, I., Widmann, M., & Vrac, M. (2017). Multi-
659 variate statistical modelling of compound events via pair-copula constructions:
660 analysis of floods in ravenna (italy). *Hydrology and Earth System Sciences*,
661 21(6), 2701–2723. Retrieved from [https://hess.copernicus.org/articles/](https://hess.copernicus.org/articles/21/2701/2017/)
662 [21/2701/2017/](https://hess.copernicus.org/articles/21/2701/2017/) doi: 10.5194/hess-21-2701-2017
- 663 Bevacqua, E., Suarez-Gutierrez, L., Jézéquel, A., Lehner, F., Vrac, M., Yiou, P., &
664 Zscheischler, J. (2023). Advancing research on compound weather and climate
665 events via large ensemble model simulations. *Nature Communications*, 14,
666 2145. Retrieved from <https://doi.org/10.1038/s41467-023-37847-5> doi:
667 10.1038/s41467-023-37847-5
- 668 Bowen, I. S. (1926). The ratio of heat losses by conduction and by evaporation from
669 any water surface. *Physical Review*, 27, 779-787.
- 670 Brunner, M. I., Seibert, J., & Favre, A.-C. (2016). Bivariate return periods and their
671 importance for flood peak and volume estimation. *WIREs Water*, 3(6), 819-
672 833. Retrieved from [https://wires.onlinelibrary.wiley.com/doi/abs/10](https://wires.onlinelibrary.wiley.com/doi/abs/10.1002/wat2.1173)
673 [.1002/wat2.1173](https://wires.onlinelibrary.wiley.com/doi/abs/10.1002/wat2.1173) doi: <https://doi.org/10.1002/wat2.1173>
- 674 Buras, A., Rammig, A., & Zang, C. S. (2020). Quantifying impacts of the 2018
675 drought on european ecosystems in comparison to 2003. *Biogeosciences*, 17(6),
676 1655–1672. Retrieved from [https://bg.copernicus.org/articles/17/1655/](https://bg.copernicus.org/articles/17/1655/2020/)
677 [2020/](https://bg.copernicus.org/articles/17/1655/2020/) doi: 10.5194/bg-17-1655-2020
- 678 Böhnisch, A., Felsche, E., & Ludwig, R. (2023). European heatwave tracks: using
679 causal discovery to detect recurring pathways in a single-regional climate
680 model large ensemble. *Environmental Research Letters*, 18(1), 014038.
681 Retrieved from <https://dx.doi.org/10.1088/1748-9326/aca9e3> doi:
682 10.1088/1748-9326/aca9e3
- 683 Böhnisch, A., Mittermeier, M., Leduc, M., & Ludwig, R. (2021). Hot spots and
684 climate trends of meteorological droughts in europe—assessing the percent of
685 normal index in a single-model initial-condition large ensemble. *Frontiers*
686 *in Water*, 3. Retrieved from [https://www.frontiersin.org/articles/](https://www.frontiersin.org/articles/10.3389/frwa.2021.716621)
687 [10.3389/frwa.2021.716621](https://www.frontiersin.org/articles/10.3389/frwa.2021.716621) doi: 10.3389/frwa.2021.716621
- 688 Ciais, P., Reichstein, N., M. and Viovy, Granier, A., Ogée, J., Allard, V., Aubinet,
689 M., ... Valentini, R. (2005). Europe-wide reduction in primary productivity
690 caused by the heat and drought in 2003. *Nature*, 437, 529–533. Retrieved from
691 <https://doi.org/10.1038/nature03972> doi: 10.1038/nature03972
- 692 Coles, S. (2001). *An introduction to statistical modeling of extreme values*. Springer
693 London.
- 694 Coles, S., Heffernan, J., & Tawn, J. (1999). Dependence measures for extreme value
695 analyses. *Extremes*, 2, 339–365. Retrieved from [https://doi.org/10.1023/](https://doi.org/10.1023/A:1009963131610)
696 [A:1009963131610](https://doi.org/10.1023/A:1009963131610) doi: 10.1023/A:1009963131610
- 697 Denissen, J. M. C., Teuling, A. J., Pitman, A. J., Koirala, S., Migliavacca, M.,
698 Li, W., ... Orth, R. (2022). Widespread shift from ecosystem energy to
699 water limitation with climate change. *Nature Climate Change*, 12, 677–
700 684. Retrieved from <https://doi.org/10.1038/s41558-022-01403-8> doi:
701 10.1038/s41558-022-01403-8
- 702 EEA, E. E. A. (2020). *Corine land cover (clc) 2018, version*
703 *2020_20u1*. ([https://land.copernicus.eu/pan-european/corine-land-](https://land.copernicus.eu/pan-european/corine-land-cover/clc2018?tab=metadata)
704 [cover/clc2018?tab=metadata](https://land.copernicus.eu/pan-european/corine-land-cover/clc2018?tab=metadata). Last accessed: 9 June 2023)
- 705 Felsche, E., Böhnisch, A., & Ludwig, R. (2023). Inter-seasonal connection of typi-
706 cal european heatwave patterns to soil moisture. *npj Climate and Atmospheric*

- 707 *Science*, 6(1), 1. doi: <https://doi.org/10.1038/s41612-023-00330-5>
- 708 Fischer, E. M., Seneviratne, S. I., Lüthi, D., & Schär, C. (2007). Contribution of
709 land-atmosphere coupling to recent european summer heat waves. *Geophysical*
710 *Research Letters*, 34(6). Retrieved from [https://agupubs.onlinelibrary](https://agupubs.onlinelibrary.wiley.com/doi/abs/10.1029/2006GL029068)
711 [.wiley.com/doi/abs/10.1029/2006GL029068](https://agupubs.onlinelibrary.wiley.com/doi/abs/10.1029/2006GL029068) doi: [https://doi.org/10.1029/](https://doi.org/10.1029/2006GL029068)
712 [2006GL029068](https://doi.org/10.1029/2006GL029068)
- 713 François, B., & Vrac, M. (2023). Time of emergence of compound events: contribu-
714 tion of univariate and dependence properties. *Natural Hazards and Earth Sys-*
715 *tem Sciences*, 23(1), 21–44. Retrieved from [https://nhess.copernicus.org/](https://nhess.copernicus.org/articles/23/21/2023/)
716 [articles/23/21/2023/](https://nhess.copernicus.org/articles/23/21/2023/) doi: 10.5194/nhess-23-21-2023
- 717 Fyfe, J. C., Derksen, C., Mudryk, L., Flato, G. M., Santer, B. D., Swart, N. C.,
718 ... Jiao, Y. (2017). Large near-term projected snowpack loss over the
719 western United States. *Nature Communications*, 8. Retrieved from
720 <https://doi.org/10.1038/ncomms14996> doi: 10.1038/ncomms14996
- 721 Gilleland, E. (2022). *extremes: Extreme value analysis. r package version 2.1-3*. Re-
722 trieved from <https://staff.ral.ucar.edu/ericg/extRemes/>
- 723 Gulev, S., Thorne, P., Ahn, J., Dentener, F., Domingues, C., Gerland, S., ... Vose,
724 R. (2021). Changing state of the climate system. In V. Masson-Delmotte et
725 al. (Eds.), *Climate change 2021: The physical science basis. contribution of*
726 *working group i to the sixth assessment report of the intergovernmental panel*
727 *on climate change*. Cambridge University Press, Cambridge, United Kingdom
728 and New York, NY, USA. doi: 10.1017/9781009157896.004
- 729 Hao, Z., Hao, F., Singh, V. P., & Zhang, X. (2018). Changes in the severity of
730 compound drought and hot extremes over global land areas. *Environment-*
731 *tal Research Letters*, 13(12), 124022. Retrieved from [https://dx.doi.org/](https://dx.doi.org/10.1088/1748-9326/aaee96)
732 [10.1088/1748-9326/aaee96](https://dx.doi.org/10.1088/1748-9326/aaee96) doi: 10.1088/1748-9326/aaee96
- 733 Hauser, M., Engelbrecht, F., & Fischer, E. M. (2022). *Transient global warming lev-*
734 *els for CMIP5 and CMIP6*. Zenodo. Retrieved from [https://doi.org/10](https://doi.org/10.5281/zenodo.7390473)
735 [.5281/zenodo.7390473](https://doi.org/10.5281/zenodo.7390473) doi: 10.5281/zenodo.7390473
- 736 Jha, S., Gudmundsson, L., & Seneviratne, S. I. (2023). Partitioning the uncertain-
737 ties in compound hot and dry precipitation, soil moisture, and runoff extremes
738 projections in cmip6. *Earth's Future*, 11(3), e2022EF003315. Retrieved
739 from [https://agupubs.onlinelibrary.wiley.com/doi/abs/10.1029/](https://agupubs.onlinelibrary.wiley.com/doi/abs/10.1029/2022EF003315)
740 [2022EF003315](https://agupubs.onlinelibrary.wiley.com/doi/abs/10.1029/2022EF003315) (e2022EF003315 2022EF003315) doi: [https://doi.org/10.1029/](https://doi.org/10.1029/2022EF003315)
741 [2022EF003315](https://doi.org/10.1029/2022EF003315)
- 742 Kirchmeier-Young, M. C., Zwiers, F. W., & Gillett, N. P. (2017). Attribution of
743 extreme events in arctic sea ice extent. *Journal of Climate*, 30(2), 553 - 571.
744 Retrieved from [https://journals.ametsoc.org/view/journals/clim/30/2/](https://journals.ametsoc.org/view/journals/clim/30/2/jcli-d-16-0412.1.xml)
745 [jcli-d-16-0412.1.xml](https://journals.ametsoc.org/view/journals/clim/30/2/jcli-d-16-0412.1.xml) doi: <https://doi.org/10.1175/JCLI-D-16-0412.1>
- 746 Kornhuber, K., Osprey, S., Coumou, D., Petri, S., Petoukhov, V., Rahmstorf, S., &
747 Gray, L. (2019). Extreme weather events in early summer 2018 connected by a
748 recurrent hemispheric wave-7 pattern. *Environmental Research Letters*, 14(5),
749 054002. Retrieved from <https://doi.org/10.1088/1748-9326/ab13bf> doi:
750 [10.1088/1748-9326/ab13bf](https://doi.org/10.1088/1748-9326/ab13bf)
- 751 Leduc, M., Mailhot, A., Frigon, A., Martel, J.-L., Ludwig, R., Brietzke, G. B.,
752 ... Scinocca, J. (2019). The climex project: A 50-member ensemble
753 of climate change projections at 12-km resolution over europe and north-
754 eastern north america with the canadian regional climate model (crcm5).
755 *Journal of Applied Meteorology and Climatology*, 58(4), 663–693. doi:
756 [10.1175/JAMC-D-18-0021.1](https://doi.org/10.1175/JAMC-D-18-0021.1)
- 757 Leonard, M., Westra, S., Phatak, A., Lambert, M., van den Hurk, B., McInnes, K.,
758 ... Stafford-Smith, M. (2014). A compound event framework for understand-
759 ing extreme impacts. *WIREs Climate Change*, 5(1), 113–128. Retrieved from
760 <https://wires.onlinelibrary.wiley.com/doi/abs/10.1002/wcc.252> doi:
761 <https://doi.org/10.1002/wcc.252>

- 762 Lesk, C., Rowhani, P., & Ramankutty, N. (2016). Influence of extreme weather
763 disasters on global crop production. *Nature*, *529*, 84–87. Retrieved from
764 <https://doi.org/10.1038/nature16467> doi: 10.1038/nature16467
- 765 Li, H., Keune, J., Smessaert, F., Nieto, R., Gimeno, L., & Miralles, D. G. (2023).
766 Land–atmosphere feedbacks contribute to crop failure in global rainfed
767 breadbaskets. *npj Climate and Atmospheric Science*, *6*, 51. Retrieved
768 from <https://doi.org/10.1038/s41612-023-00375-6> doi: 10.1038/
769 s41612-023-00375-6
- 770 Liu, P. R., & Raftery, A. E. (2021). Country-based rate of emissions reduc-
771 tions should increase by 80% beyond nationally determined contributions
772 to meet the 2 °c target. *Communications Earth & Environment*, *2*, 29.
773 Retrieved from <https://doi.org/10.1038/s43247-021-00097-8> doi:
774 10.1038/s43247-021-00097-8
- 775 Maher, N., Milinski, S., & Ludwig, R. (2021). Large ensemble climate model
776 simulations: introduction, overview, and future prospects for utilising multi-
777 ple types of large ensemble. *Earth System Dynamics*, *12*(2), 401–418. Re-
778 trieved from <https://esd.copernicus.org/articles/12/401/2021/> doi:
779 10.5194/esd-12-401-2021
- 780 Manning, C., Widmann, M., Bevacqua, E., Loon, A. F. V., Maraun, D., & Vrac, M.
781 (2019). Increased probability of compound long-duration dry and hot events in
782 europe during summer (1950–2013). *Environmental Research Letters*, *14*(9),
783 094006. Retrieved from <https://dx.doi.org/10.1088/1748-9326/ab23bf>
784 doi: 10.1088/1748-9326/ab23bf
- 785 Markonis, Y., Kumar, R., Hanel, M., Rakovec, O., Máca, P., & AghaKouchak, A.
786 (2021). The rise of compound warm-season droughts in europe. *Science Ad-
787 vances*, *7*(6), eabb9668. Retrieved from [https://www.science.org/doi/abs/
788 10.1126/sciadv.abb9668](https://www.science.org/doi/abs/10.1126/sciadv.abb9668) doi: 10.1126/sciadv.abb9668
- 789 Miller, J., Böhnisch, A., Ludwig, R., & Brunner, M. I. (2023). Climate change im-
790 pacts on regional fire weather in heterogeneous landscapes of central europe.
791 *Natural Hazards and Earth System Sciences Discussions*, *2023*, 1–25. Re-
792 trieved from [https://nhess.copernicus.org/preprints/nhess-2023-51/
793 doi: 10.5194/nhess-2023-51](https://nhess.copernicus.org/preprints/nhess-2023-51/)
- 794 Miralles, D. G., Gentile, P., Seneviratne, S. I., & Teuling, A. J. (2019).
795 Land–atmospheric feedbacks during droughts and heatwaves: state of the
796 science and current challenges. *Annals of the New York Academy of Sci-
797 ences*, *1436*(1), 19–35. Retrieved from [https://nyaspubs.onlinelibrary
798 .wiley.com/doi/abs/10.1111/nyas.13912](https://nyaspubs.onlinelibrary.wiley.com/doi/abs/10.1111/nyas.13912) doi: [https://doi.org/10.1111/
799 nyas.13912](https://doi.org/10.1111/nyas.13912)
- 800 Mukherjee, S., & Mishra, A. K. (2021). Increase in compound drought and
801 heatwaves in a warming world. *Geophysical Research Letters*, *48*(1),
802 e2020GL090617. Retrieved from [https://agupubs.onlinelibrary.wiley
803 .com/doi/abs/10.1029/2020GL090617](https://agupubs.onlinelibrary.wiley.com/doi/abs/10.1029/2020GL090617) (e2020GL090617 2020GL090617) doi:
804 <https://doi.org/10.1029/2020GL090617>
- 805 Mukherjee, S., Mishra, A. K., Zscheischler, J., & Entekhabi, D. (2023). Interac-
806 tion between dry and hot extremes at a global scale using a cascade modeling
807 framework. *Nature Communications*, *14*, 277. Retrieved from [https://
808 doi.org/10.1038/s41467-022-35748-7](https://doi.org/10.1038/s41467-022-35748-7) doi: 10.1038/s41467-022-35748-7
- 809 Nagler, T., Schepsmeier, U., Stoeber, J., Brechmann, E. C., Graeler, B., Erhardt,
810 T., . . . Vatter, T. (2023). *Vinecopula: Statistical inference of vine copulas.
811 r package version 2.4.5*. Retrieved from [https://github.com/tnagler/
812 VineCopula](https://github.com/tnagler/VineCopula)
- 813 O, S., Bastos, A., Reichstein, M., Li, W., Denissen, J., Graefen, H., & Orth, R.
814 (2022). The role of climate and vegetation in regulating drought–heat ex-
815 tremes. *Journal of Climate*, *35*(17), 5677–5685. Retrieved from [https://
816 journals.ametsoc.org/view/journals/clim/35/17/JCLI-D-21-0675.1.xml](https://journals.ametsoc.org/view/journals/clim/35/17/JCLI-D-21-0675.1.xml)

- 817 doi: <https://doi.org/10.1175/JCLI-D-21-0675.1>
- 818 Poschlod, B., Zscheischler, J., Sillmann, J., Wood, R. R., & Ludwig, R. (2020). Cli-
819 mate change effects on hydrometeorological compound events over southern
820 norway. *Weather and Climate Extremes*, *28*, 100253. Retrieved from [https://](https://www.sciencedirect.com/science/article/pii/S2212094719301574)
821 www.sciencedirect.com/science/article/pii/S2212094719301574 doi:
822 <https://doi.org/10.1016/j.wace.2020.100253>
- 823 Richardson, M. I., Cowtan, K. D., Hawkins, E., & Stolpe, M. B. (2016). Rec-
824 onciled climate response estimates from climate models and the energy
825 budget of earth. *Nature Climate Change*, *6*, 931-935. Retrieved from
826 <https://doi.org/10.1038/nclimate3066> doi: 10.1038/nclimate30660
- 827 Rousi, E., Fink, A. H., Andersen, L. S., Becker, F. N., Beobide-Arsuaga, G., Breil,
828 M., ... Xoplaki, E. (2023). The extremely hot and dry 2018 summer in central
829 and northern europe from a multi-faceted weather and climate perspective.
830 *Natural Hazards and Earth System Sciences*, *23*(5), 1699–1718. Retrieved
831 from <https://nhess.copernicus.org/articles/23/1699/2023/> doi:
832 10.5194/nhess-23-1699-2023
- 833 Salvadori, G., Durante, F., De Michele, C., Bernardi, M., & Petrella, L. (2016). A
834 multivariate copula-based framework for dealing with hazard scenarios and
835 failure probabilities. *Water Resources Research*, *52*(5), 3701-3721. Retrieved
836 from [https://agupubs.onlinelibrary.wiley.com/doi/abs/10.1002/](https://agupubs.onlinelibrary.wiley.com/doi/abs/10.1002/2015WR017225)
837 [2015WR017225](https://agupubs.onlinelibrary.wiley.com/doi/abs/10.1002/2015WR017225) doi: <https://doi.org/10.1002/2015WR017225>
- 838 Schwalm, C. R., Glendon, S., & Duffy, P. B. (2020). Rcp8.5 tracks cumulative
839 co₂ emissions. *Proceedings of the National Academy of Sciences*,
840 *117*(33), 19656-19657. Retrieved from [https://www.pnas.org/doi/abs/](https://www.pnas.org/doi/abs/10.1073/pnas.2007117117)
841 [10.1073/pnas.2007117117](https://www.pnas.org/doi/abs/10.1073/pnas.2007117117) doi: 10.1073/pnas.2007117117
- 842 Schwingshackl, C., Hirschi, M., & Seneviratne, S. I. (2017). Quantifying spa-
843 tiotemporal variations of soil moisture control on surface energy balance and
844 near-surface air temperature. *Journal of Climate*, *30*(18), 7105 - 7124. Re-
845 trieved from [https://journals.ametsoc.org/view/journals/clim/30/18/](https://journals.ametsoc.org/view/journals/clim/30/18/jcli-d-16-0727.1.xml)
846 [jcli-d-16-0727.1.xml](https://journals.ametsoc.org/view/journals/clim/30/18/jcli-d-16-0727.1.xml) doi: <https://doi.org/10.1175/JCLI-D-16-0727.1>
- 847 Seneviratne, S., Zhang, X., Adnan, M., Badi, W., Dereczynski, C., Di Luca, A., ...
848 Zhou, B. (2021). Weather and climate extreme events in a changing climate.
849 In V. Masson-Delmotte et al. (Eds.), *Climate change 2021: The physical sci-*
850 *ence basis. contribution of working group i to the sixth assessment report of the*
851 *intergovernmental panel on climate change*. doi: 10.1017/9781009157896.013
- 852 Swart, N. C., Cole, J. N. S., Kharin, V. V., Lazare, M., Scinocca, J. F., Gillett,
853 N. P., ... Winter, B. (2019). The canadian earth system model version 5
854 (canesm5.0.3). *Geoscientific Model Development*, *12*(11), 4823–4873. Re-
855 trieved from <https://gmd.copernicus.org/articles/12/4823/2019/> doi:
856 10.5194/gmd-12-4823-2019
- 857 Teuling, A. J., Hirschi, M., Ohmura, A., Wild, M., Reichstein, M., Ciais, P., ...
858 Seneviratne, S. I. (2009). A regional perspective on trends in continental
859 evaporation. *Geophysical Research Letters*, *36*(2). Retrieved from [https://](https://agupubs.onlinelibrary.wiley.com/doi/abs/10.1029/2008GL036584)
860 agupubs.onlinelibrary.wiley.com/doi/abs/10.1029/2008GL036584 doi:
861 <https://doi.org/10.1029/2008GL036584>
- 862 Toreti, A., Belward, A., Perez-Dominguez, I., Naumann, G., Luterbacher, J., Cronie,
863 O., ... Zampieri, M. (2019). The exceptional 2018 european water seesaw
864 calls for action on adaptation. *Earth's Future*, *7*(6), 652-663. Retrieved
865 from [https://agupubs.onlinelibrary.wiley.com/doi/abs/10.1029/](https://agupubs.onlinelibrary.wiley.com/doi/abs/10.1029/2019EF001170)
866 [2019EF001170](https://agupubs.onlinelibrary.wiley.com/doi/abs/10.1029/2019EF001170) doi: <https://doi.org/10.1029/2019EF001170>
- 867 Trenberth, K. E., & Shea, D. J. (2005). Relationships between precipitation and
868 surface temperature. *Geophysical Research Letters*, *32*(14). Retrieved
869 from [https://agupubs.onlinelibrary.wiley.com/doi/abs/10.1029/](https://agupubs.onlinelibrary.wiley.com/doi/abs/10.1029/2005GL022760)
870 [2005GL022760](https://agupubs.onlinelibrary.wiley.com/doi/abs/10.1029/2005GL022760) doi: <https://doi.org/10.1029/2005GL022760>
- 871 UNFCCC. (2015). *Adoption of the paris agreement. report no.*

- 872 *fccc/cp/2015/l.9/rev.1*. Retrieved from [http://unfccc.int/resource/](http://unfccc.int/resource/docs/2015/cop21/eng/109r01.pdf)
873 [docs/2015/cop21/eng/109r01.pdf](http://unfccc.int/resource/docs/2015/cop21/eng/109r01.pdf)
- 874 Vogel, M. M., Zscheischler, J., Wartenburger, R., Dee, D., & Seneviratne, S. I.
875 (2019). Concurrent 2018 hot extremes across northern hemisphere due to
876 human-induced climate change. *Earth's Future*, 7(7), 692-703. Retrieved
877 from [https://agupubs.onlinelibrary.wiley.com/doi/abs/10.1029/](https://agupubs.onlinelibrary.wiley.com/doi/abs/10.1029/2019EF001189)
878 [2019EF001189](https://doi.org/10.1029/2019EF001189) doi: <https://doi.org/10.1029/2019EF001189>
- 879 von Trentini, F., Leduc, M., & Ludwig, R. (2019). Assessing natural variability
880 in RCM signals: comparison of a multi model EURO-CORDEX ensemble
881 with a 50-member single model large ensemble. *Climate Dynamics*, 53, 1963-
882 1979. Retrieved from <https://doi.org/10.1007/s00382-019-04755-8> doi:
883 [10.1007/s00382-019-04755-8](https://doi.org/10.1007/s00382-019-04755-8)
- 884 Wang, R., Lü, G., Ning, L., Yuan, L., & Li, L. (2021). Likelihood of compound
885 dry and hot extremes increased with stronger dependence during warm
886 seasons. *Atmospheric Research*, 260, 105692. Retrieved from [https://](https://www.sciencedirect.com/science/article/pii/S0169809521002489)
887 www.sciencedirect.com/science/article/pii/S0169809521002489 doi:
888 <https://doi.org/10.1016/j.atmosres.2021.105692>
- 889 Zink, M., Samaniego, L., Kumar, R., Thober, S., Mai, J., Schäfer, D., & Marx, A.
890 (2016). The german drought monitor. *Environmental Research Letters*, 11(7),
891 074002. Retrieved from [https://dx.doi.org/10.1088/1748-9326/11/7/](https://dx.doi.org/10.1088/1748-9326/11/7/074002)
892 [074002](https://dx.doi.org/10.1088/1748-9326/11/7/074002) doi: [10.1088/1748-9326/11/7/074002](https://dx.doi.org/10.1088/1748-9326/11/7/074002)
- 893 Zscheischler, J., & Fischer, E. M. (2020). The record-breaking compound hot and
894 dry 2018 growing season in germany. *Weather and Climate Extremes*, 29,
895 100270. Retrieved from [https://www.sciencedirect.com/science/article/](https://www.sciencedirect.com/science/article/pii/S2212094719302002)
896 [pii/S2212094719302002](https://www.sciencedirect.com/science/article/pii/S2212094719302002) doi: <https://doi.org/10.1016/j.wace.2020.100270>
- 897 Zscheischler, J., Martius, O., Westra, S., Bevacqua, E., Raymond, C., Horton,
898 R. M., ... Vignotto, E. (2020). A typology of compound weather and
899 climate events. *Nature Reviews Earth & Environment*, 1, 333-347. Re-
900 trieved from <https://doi.org/10.1038/s43017-020-0060-z> doi:
901 [10.1038/s43017-020-0060-z](https://doi.org/10.1038/s43017-020-0060-z)
- 902 Zscheischler, J., Orth, R., & Seneviratne, S. I. (2015). A submonthly database
903 for detecting changes in vegetation-atmosphere coupling. *Geophysical*
904 *Research Letters*, 42(22), 9816-9824. Retrieved from [https://agupubs](https://agupubs.onlinelibrary.wiley.com/doi/abs/10.1002/2015GL066563)
905 [.onlinelibrary.wiley.com/doi/abs/10.1002/2015GL066563](https://agupubs.onlinelibrary.wiley.com/doi/abs/10.1002/2015GL066563) doi:
906 <https://doi.org/10.1002/2015GL066563>
- 907 Zscheischler, J., & Seneviratne, S. I. (2017). Dependence of drivers affects risks as-
908 sociated with compound events. *Science Advances*, 3(6), e1700263. Retrieved
909 from <https://www.science.org/doi/abs/10.1126/sciadv.1700263> doi: [10](https://www.science.org/doi/abs/10.1126/sciadv.1700263)
910 [.1126/sciadv.1700263](https://www.science.org/doi/abs/10.1126/sciadv.1700263)

1 **Future hotspots of compound dry and hot summers**
2 **emerge in European agricultural areas**

3 **Andrea Böhnisch¹, Elizaveta Felsche^{1,2}, Magdalena Mittermeier¹, Benjamin**
4 **Poschlod³, Ralf Ludwig¹**

5 ¹Department of Geography, Ludwig-Maximilians-Universität München, Munich, Germany

6 ²Center for Digital Technology and Management, Munich, Germany

7 ³Research Unit Sustainability and Climate Risk, Center for Earth System Research and Sustainability,
8 Universität Hamburg, Hamburg, Germany

9 **Key Points:**

- 10 • During compound dry and hot extreme (CDHE) summers, latent heat flux is markedly
11 reduced in widespread areas of the European continent.
- 12 • The frequency increase of CDHE events, associated with extremely low soil mois-
13 ture, doubles under GWL3 compared to GWL2.
- 14 • CDHE frequency increases are predominantly driven by rising temperature, with
15 regional contributions of bivariate tail dependence increases.

Corresponding author: Andrea Böhnisch, a.boehnisch@lmu.de

Abstract

Compound dry and hot extremes (CDHE, such as recent summers 2015, 2018 and 2022 in Europe) have wide ranging impacts: Heat exacerbates moisture shortages during dry periods whereas water demand rises. Climate change will likely increase the intensity, frequency, and duration of CDHE events in Europe. However, current studies focus on drivers and impacts in coarse-resolution global climate models and likely miss spatial details of CDHE characteristics. To overcome this issue, we exploit a regional 50-member single-model initial condition large ensemble (SMILE) at 12 km spatial resolution. Hence 1000 model years per 20 year-periods provide an extensive database of CDHE and robust estimations of their occurrence changes across Europe in high geographical detail. CDHE occurrences are investigated in a current climate and at two global warming levels (+2 °C, +3 °C). We identify Northern France, Southern Germany, Switzerland, Southern Ireland, and the western coasts of the Black Sea with currently low CDHE frequencies as emerging hotspots. These regions experience a tenfold occurrence increase under global warming conditions. Apart from Western Europe, temperature is the dominant contributor to frequency increases. Furthermore, tail dependencies strengthen in regions with high CDHE frequency increases. In European agricultural areas, soil moisture shows very strong negative correlations with CDHE extremeness. Last, our results suggest a halving of CDHE in a +2 °C world compared to a +3 °C world, highlighting the necessity of climate mitigation with respect to this hazard type.

Plain Language Summary

During the last years, summers tended to be exceptionally dry and hot at the same time. Dry and hot conditions affect various economic and ecologic sectors, for example agriculture by soil moisture reduction. Assessing their frequency and intensity under climate change conditions is hence pivotal to develop effective adaptation strategies. The particularity of this study is a so-called regional climate model large ensemble: Its 50 simulations from the same model are equally probable realizations of climate trajectories. We thus investigate 1000 model years for a current climate, a +2°C and +3°C warmer world at high geographical detail. This allows for robust analysis as numerous events occur per period. We show that hot and dry summers become more frequent, mostly because of warming with some regions affected by both warming and drying. Furthermore, we find a strengthening link between high temperature and low precipitation, which is often not considered in studies. Additionally, lower soil moisture conditions in agricultural areas coincide with more extreme dry and hot summers. In a +3°C world, these events are projected to occur at least twice as frequent as in a +2°C world. This stresses the relevance of climate change mitigation efforts.

1 Introduction

Triggered by an accumulation of recent events, the temporal co-occurrence of extremely dry and hot conditions has sparked a large literature body. Globally, but especially in Europe, simultaneous droughts and heatwaves rank first among multivariate hazard investigations (Afroz et al., 2023). Up to 20 % of heatwaves coincided with droughts since the 1980s (rising trend; Mukherjee & Mishra, 2021). In Europe, droughts during the warm season – often accompanied by heatwaves – increasingly emerge as the dominant drought type (Markonis et al., 2021). For instance, the year 2018 exhibited unprecedented dry and hot conditions during spring to summer in the northern hemisphere (Buras et al., 2020). Vegetation, thriving from suitable growing conditions in spring, aggravated soil depletion by summer due to enhanced transpiration (Bastos et al., 2020).

Heatwaves and droughts share common drivers, albeit on different effective time scales (Miralles et al., 2019). This is reflected in the general negative correlation of temperature and precipitation (Zscheischler & Fischer, 2020; Trenberth & Shea, 2005). For

66 example, in 2018 anticyclonic blocking through April–October over central Europe, in
67 particular a stationary pattern that was recurrently associated with heat anomalies over
68 Europe and North America, favored persistent dry and hot conditions (Buras et al., 2020;
69 Toreti et al., 2019; Rousi et al., 2023; Kornhuber et al., 2019). Buras et al. (2020) also
70 show the close spatial correspondence of high pressure, hot extremes (which typically oc-
71 cur below anticyclonic conditions, Kornhuber et al., 2019), and water budget deficits.
72 This context can be explained by drying and warming in descending air masses, which
73 exacerbate atmospheric evaporative demand such that subsequently increased evapotran-
74 spiration may reduce soil moisture (e.g., Zscheischler et al., 2020). Dry soils in turn heat
75 up more quickly and thus support the sensible heat flux (e.g., Schwingshackl et al., 2017).
76 The warming effect in humid areas during hot and dry conditions due to enhanced net
77 radiation is dampened by evaporative cooling, which is induced by vegetation transpi-
78 ration and soil evaporation (O et al., 2022). In arid areas, generally low soil water con-
79 tents and dry vegetation constrain latent heat and amplify temperature increases via en-
80 hanced sensible heat fluxes (O et al., 2022). Locally, drought conditions precede extreme
81 heat in summers (Felsche et al., 2023), while simultaneous drought conditions may pro-
82 long heatwaves via land-atmospheric coupling (Fischer et al., 2007).

83 This relationship is mutual: Manning et al. (2019) suggest that enduring and in-
84 tense hot and dry conditions also trigger soil moisture droughts, and Mukherjee et al.
85 (2023) find amplifying soil effects in both drought–heat and heat–drought cascades. In
86 Germany, soil moisture depletion and precipitation deficits during summer 2018 resulted
87 in a shift from commonly energy-limited to moisture-limited evaporative regimes (Rousi
88 et al., 2023). Soil moisture deficits, however, considerably hamper vegetation produc-
89 tivity (Bastos et al., 2020). In summer 2018, the general water budget was more strongly
90 affected in European agricultural and pasture regions than in forests, but vegetation de-
91 graded in both arable and forest regions (Buras et al., 2020). Crop yields of major plants
92 in Northern and central Europe were halved compared to the preceding 5 years (Toreti
93 et al., 2019). In the similarly hot and dry summer of 2003, European gross and net pri-
94 mary production decreased by up to 30 % and 20 %, respectively (Ciais et al., 2005). While
95 heat was shown to mostly affect crop yields, droughts additionally kill the plants (Lesk
96 et al., 2016). Thus a co-occurrence of both extremes also bears the potential to merge
97 impacts, especially by affecting soil moisture as a pre-condition for crop development.

98 The impacts of compounding extremes are hence amplified compared to its single
99 components. This holds also true for compound dry and hot extreme (CDHE) events,
100 as mentioned previously. Literature describes various kinds of compound events, e.g., pre-
101 conditioned, temporally or spatially compounding, and multivariate types (e.g., Zscheis-
102 chler et al., 2020). CDHE can be considered as multivariate, in that two hazards co-occur
103 simultaneously in time and space due to their common drivers, or as pre-conditioned if,
104 e.g., soil moisture conditions of previous seasons were taken into account (Zscheischler
105 et al., 2020). Identifying compound events with joint distributions, in this case of tem-
106 perature and precipitation, allows their investigation via multivariate probability distri-
107 bution functions, i.e., copulas (Bevacqua et al., 2017; Zscheischler et al., 2020). These
108 represent dependencies among the variables and can be used to derive multivariate ex-
109 treme value probabilities (Zscheischler et al., 2020). Event occurrence probabilities in
110 turn can be expressed as return periods. For instance, return periods for the CDHE grow-
111 ing season 2018 exceed several thousand years for certain event definitions (Zscheischler
112 & Fischer, 2020). Especially in situations where adaptation and decision making rely on
113 return periods, such as water resources management, bivariate analyses are essential. With-
114 out considering the bivariate dependence structure, there is a risk of both overestimat-
115 ing or underestimating the occurrence of events (Bevacqua et al., 2017): For instance,
116 bivariate return periods of the 2014 California winter drought, one of the first CDHE to
117 be investigated bivariately, were shown to be higher than univariate precipitation deficit
118 return periods owing to extremely high winter temperatures (AghaKouchak et al., 2014).

Most studies on bivariate events focus on prominent cases without gaining generalized knowledge on the event–impact relationships by, e.g., aligning event extremeness with impact extremeness. Examples for this approach include the calculation of (standardized) temperature and precipitation ratios or products (Hao et al., 2018; Mukherjee & Mishra, 2021), but without considering the variable dependencies. Others employ water budget deficits as CDHE intensity surrogate (Buras et al., 2020). In this study, we consider bivariate return periods as an intensity surrogate. Since they indicate the joint extremeness of the considered variables, higher return periods also correspond to higher temperatures and lower precipitation in the CDHE case. To illustrate the intensity of the bivariate return periods, we align soil moisture to the CDHE.

In order to evaluate low-frequency compound events and derive meaningful knowledge on their effects on soil moisture, observational records provide too few events. Hence, ensembles of climate model simulations are beneficial to enlarge the event sample. However, for the investigation of compound events, it is advisable to be sure about comparable process representation in all used simulations (e.g., regarding the joint temperature–precipitation distribution). Both issues can be addressed by accessing single-model initial condition large ensembles (SMILEs) (e.g., Maher et al., 2021). SMILEs consist of several simulations of the same model under the same external forcing conditions (i.e., scenario), differing only due to their initial conditions. Global SMILEs proved to be a skillful tool for the reduction of uncertainty due to internal variability in multivariate event attribution (Bevacqua et al., 2023). However, it is a known issue that compound events require finer spatial resolution if realistic information for adaptation planning on a regional scale is sought (François & Vrac, 2023).

The goal of this study is thus to (a) obtain and explain spatially explicit frequency changes in European CDHE summers (June–August, JJA) under three global warming levels and (b) relate the ranked events with soil moisture as a relevant condition for impacts on agriculture. In order to reduce sampling uncertainties from a statistical perspective and address internal climate variability, we employ a regional high resolution SMILE.

2 Materials and Methods

2.1 Regional Large Ensemble Data for robust sampling

Investigating low-probability compound events of extremes requires an abundant data base. We therefore employ the regional SMILE of the Canadian Regional Climate Model, version 5 (CRCM5-LE; Leduc et al., 2019). The CRCM5-LE was developed within the ClimEx project: 50 members of the Canadian Earth System Model, version 2, Large Ensemble (CanESM2-LE; Fyfe et al., 2017; Kirchmeier-Young et al., 2017) were dynamically downscaled with the CRCM5 to obtain 50 high-resolution (0.11° , corresponding to 12.5 km) time series of 1950–2099 over two domains, Europe and Northeastern North America (Leduc et al., 2019). The original members of the CanESM2-LE were constructed by applying small random perturbations to the long-term control run in 1850 and subsequently in 1950. After a few years, the 50 members are considered to be independent due to the chaotic nature of weather sequences, while still following the same forcing conditions (RCP8.5 from 2006 onward) and thus pertaining comparable climate statistics (Leduc et al., 2019).

The CRCM5-LE already proved its value for compound analyses of hydro-meteorological extremes, namely rain on saturated soil and rain-on-snow events (Poschod et al., 2020). Further, this regional SMILE was used for investigation of heatwaves (Böhnisch et al., 2023), droughts (Böhnisch et al., 2021), and heat and drought linkage at an inter-seasonal scale (Felsche et al., 2023).

168 2.2 Global Warming Levels in a regional climate model

169 We employed global warming levels (GWL) for our analysis of future climate pro-
 170 jections. This approach has been widely applied because it has the advantage of being
 171 less sensitive to the selected model and scenario. Furthermore, it allows to directly com-
 172 pare the warming rate to the goal of the Paris Agreement of limiting global warming to
 173 “(...) well below 2 °C above pre-industrial levels and to pursue efforts to limit the tem-
 174 perature increase to 1.5 °C (...)” (UNFCCC, 2015). The GWLs were calculated as anoma-
 175 lies in the yearly global mean surface air temperature (*tas*) to the pre-industrial refer-
 176 ence period 1850–1900 (Hauser et al., 2022; Seneviratne et al., 2021). GWLs refer to a
 177 20-year period centered around the first year, in which the warming level is exceeded (tas
 178 $>$ GWL). The methodology is based on Hauser et al. (2022), which was used for the Sixth
 179 Assessment Report of the Intergovernmental Panel on Climate Change (IPCC). We adopted
 180 the code for the use in the CanESM2-LE. To this end, we pooled all 50 members before
 181 calculating the anomalies to 1850–1900.

182 Our reference period 2001–2020 translates to $GWL = +1.2$ °C (GWL1.2) in CanESM2-
 183 LE (observed approximately 1 °C; Gulev et al., 2021). This is less an effect of the forc-
 184 ing scenario for RCP8.5 was shown to be in high agreement with observed emissions (Schwalm
 185 et al., 2020). Instead, it mirrors the model’s rather high equilibrium climate sensitivity
 186 (3.7 K; Swart et al., 2019). Comparing modeled global *tas* with observational global mean
 187 temperature though may result in an overestimation partly due to insufficient observa-
 188 tional data coverage and blending air temperature over land with sea surface temper-
 189 atures over ocean areas in observations (Richardson et al., 2016; Vogel et al., 2019).

190 Future periods in our study are represented by 20-year slices centered at $GWL =$
 191 $+2$ °C (GWL2, Paris Agreement; UNFCCC, 2015) and $GWL = +3$ °C (GWL3, close to
 192 the most realistic end-of-century temperature of 2.8 °C under current trends in climate
 193 policy; Liu & Raftery, 2021).

194 Time periods corresponding to a given GWL were calculated within the global SMILE,
 195 and adopted for use in the regional SMILE.

196 2.3 Definition and Bivariate Evaluation of Compound Events

197 2.3.1 Event Definition

198 This study takes a multivariate perspective on dry and hot extremes, since we are
 199 particularly interested in the combined occurrences of these hazards. We employed thus
 200 the “AND” hazard scenario to connect both univariate extremes (Zscheischler & Fischer,
 201 2020): the temporal co-occurrence of linearly detrended summer mean temperatures and
 202 (negative) precipitation sums exceeding the respective 95th percentile of 2001–2020 (with
 203 the 95th percentile of negative precipitation equaling the 5th percentile; see Supplemen-
 204 tary figure S1). By definition, these events are expected to be very rare because both
 205 variables have to exceed a high threshold. However, since JJA temperature and nega-
 206 tive precipitation show strong correlations in most parts of Europe, which intensified dur-
 207 ing the 21st century, CDHE occur more often than would be implied by independence
 208 (Zscheischler & Seneviratne, 2017). This implies that warm summers are commonly dry
 209 and wet summers are cool (see also Trenberth & Shea, 2005; Wang et al., 2021). Due
 210 to the extensive large ensemble database, 1000 years instead of 20 years (see fig. 1 (a))
 211 are available per analysis period and allow for robust baseline definition (i.e., percentile
 212 estimates across all 50 ensemble members) and event characteristic estimation (e.g., fre-
 213 quency changes, associated behavior).

214 In order to characterize CDHE summer energy partitioning compared to non-CDHE
 215 summers, we employed the Bowen Ratio (BR, Bowen, 1926). The BR describes the ra-
 216 tio of sensible heat flux and latent heat flux, which are negatively coupled (e.g., Schwing-

shackl et al., 2017). For this analysis, we used the model variables surface upward latent heat flux and surface upward sensible heat flux.

2.3.2 Estimation of Bivariate Return Periods

In order to estimate the joint extremeness of CDHEs, we calculated bivariate return periods. Generally, return periods are the inverse of the (annual) exceedance probability p of a given event intensity, the return level z_p . Hence, the return level z_p is expected to be exceeded every $1/p$ years, defining thus the return period $T = 1/p$ (Coles, 2001). Bivariate return periods however remain ambiguous and become larger than their univariate component return periods due to the second variable that is required to meet the extremes condition as well (AghaKouchak et al., 2014; Zscheischler & Fischer, 2020). In large samples like the CRCM5-LE, (annual) event occurrences per time period can be counted and inverted to obtain the return period (Zscheischler & Fischer, 2020). This empirical approach is generally limited by the time series length. With 1000 years available, 10 events with $T = 100$ are to be expected statistically, while the most extreme case would be $T = 1000$. Any inference on this level would be highly uncertain since it is based on a single event (e.g., Zscheischler & Fischer, 2020). For shorter time series, the maximum empirical T also decreases such that extreme event estimation suffers from high uncertainties (Bevacqua et al., 2017). Instead of event counting, we here fitted copulas, i.e., multivariate probability distributions, to the bivariate distributions (Zscheischler & Fischer, 2020). The large advantage of distribution fitting is the option for pushing the rareness boundaries of the empirical approach.

For the procedure in this study we used the R package *VineCopula* (Nagler et al., 2023). First, we transformed the empirical marginals of summer temperature and precipitation (multiplied with -1 for calculation purposes) to uniform distributions on $[0,1]$. Next, the most suitable copula family was estimated using the Bayesian Information Criterion (BIC) and fitted to the data. For this study, we chose the locally best fitting copula family from eight single-parametric copula families (fig. S3).

Following the relation in Brunner et al. (2016), the return period T was obtained by:

$$T(u, v) = \frac{\mu}{1 - u - v + C(u, v)} \quad (1)$$

giving the probability for jointly exceeding the event defining thresholds in the denominator, with u, v corresponding to univariate probabilities of exceeding the respective threshold, $C(u, v)$ being the copula at (u, v) , and the mean interarrival time $\mu = 1$ in our case since we investigated annual events (Zscheischler & Fischer, 2020; Zscheischler & Seneviratne, 2017; Brunner et al., 2016).

2.3.3 Distributional Change Assessments

Both changes in temperature and precipitation may lead to frequency changes by shifting the bivariate distribution compared to the reference period. Additionally, the bivariate (tail) dependence structure may change over time.

In order to address the first point, we here propose a method to disentangle the dominating drivers of frequency changes. Horizontal shifts of the distribution (along the orange line in fig. 1 (b)) indicate temperature changes as sole drivers whereas vertical shifts (along the blue line in fig. 1 (b)) point to precipitation changes. Any change with both a horizontal and vertical component thus is due to a combination of temperature and precipitation changes. For the definition of the dominating driver, we used the average JJA drying per degree warming (fig. 1 (b)): In Europe, the slope of this relation-

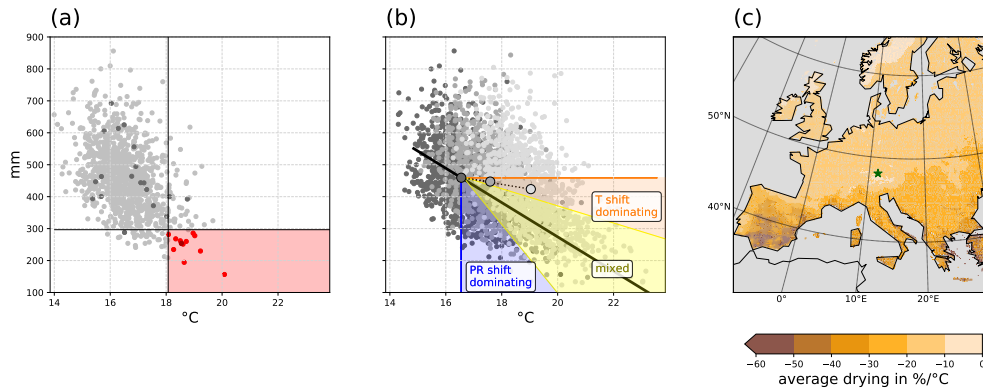


Figure 1. (a) Precipitation and temperature of 1000 summers (50 members for 2001–2020) over a grid cell representing Munich/Germany (star in (c)). Dark grey and dark red dots show the limited sample of one arbitrary member. Black lines indicate the 95th percentile of temperature (vertical) and 5th percentile of precipitation (i.e., the 95th percentile of negative precipitation; horizontal) with the red area highlighting all summers meeting the definition criterion for a CDHE. (b) Definition of temperature (orange) and precipitation (blue) dominance in distributional shifts under climate change conditions. Yellow indicates mixed contributions of temperature and precipitation (see text). Grey shaded point clouds correspond to current, GWL2, and GWL3 climates for the same pixel as in (a). The black line represents the local average summer drying scaled with warming. (c) Average summer drying scaled with warming expressed as slopes of a linear line fitted to the local bivariate distribution.

262 ship follows a North–South gradient with highest values in the Mediterranean area and
 263 especially over the Iberian Peninsula where summer precipitation is very low (fig. 1 (c)).
 264 Distributional shifts along this slope represent the occurrence of more extreme events
 265 by heating and drying following the current relationship. If the center of the distribu-
 266 tion is shifted within the orange sector of fig. 1 (b), temperature is identified as dom-
 267 inating driver, while it is precipitation for shifts into the blue sector. Since we are also
 268 interested in simultaneous changes of temperature and precipitation, we introduced a
 269 buffer zone between a line with half the local slope and a line with twice the local slope
 270 to account for uncertainties in slope estimation (yellow sector). This combination is fur-
 271 ther referred to as mixed drivers. This approach is based on correlation of the full dis-
 272 tributions, which, as Zscheischler and Seneviratne (2017) argue, can serve as an indica-
 273 tor for the likelihood of CDHE if the percentile threshold for event definition is not too
 274 high.

275 To account for dependencies in the distribution extremes, tail (= extremal) depen-
 276 dence above the 95th univariate percentiles ($\chi(0.95)$; Coles et al., 1999) were cal-
 277 culated for each period separately using the R package *extRemes* (Gilleland, 2022). Con-
 278 fidence intervals at the 0.05 level were obtained by bootstrapping 1000 times.

279 2.4 Assessment of CDHE Impacts on Soil Moisture

280 In one of the first compound event definitions by Leonard et al. (2014), compound
 281 events are defined by the extremeness of impacts originating from multiple contribut-
 282 ing hazards. While our CDHE definition rather follows a hazard-based perspective, we
 283 nevertheless aim to assess CDHE effects in this study. Our (univariate) target variable
 284 is soil moisture, classified as the soil moisture index (SMI) of Zink et al. (2016), which
 285 also forms the basis of the German Drought Monitor. The SMI is based on soil mois-

286 ture percentiles of a reference period (2001–2020 in our case). We used JJA soil mois-
 287 ture in the upper portion of the soil column to assess agricultural droughts during cur-
 288 rent climate, GWL2, and GWL3. Soil moisture is especially useful when assessing event
 289 impacts, for soil moisture droughts have large agricultural and ecosystem-specific impacts.
 290 Assessing soil moisture conditions is hence most relevant in areas where they potentially
 291 have an impact. Therefore, we confined our analyses of CDHE–soil moisture relation-
 292 ships on European agricultural areas. These comprise Corine Land Cover (CLC2018 ver-
 293 sion 2020_20u1, linearly regridded to CRCM5-LE spatial resolution; EEA, 2020) level-
 294 2 classes *arable land*, *permanent crops*, and *heterogeneous agricultural areas*.

295 3 Results

296 3.1 Bowen Ratio Increases During CDHE

297 CDHE and non-CDHE summers differ with respect to the energy-partitioning of
 298 sensible and latent heat flux. In order to illustrate these differences in a spatially explicit
 299 way, we first look at the Bowen Ratio during summer under current climate conditions.
 300 During non-CDHE summers, the latent heat flux, i.e., evaporative cooling (O et al., 2022),
 301 is dominating over the sensible heat flux in large areas of Europe (fig. 2 (a)–(b)). These
 302 coincide with the wet evapotranspiration regions (energy-limited) of Schwingshackl et
 303 al. (2017). The dominating low BR conditions favor widespread cloud formation and sum-
 304 mer precipitation. In CDHE summers (fig. 2 (b)), however, BR increases in large areas.
 305 High BR occurs in their wet/transition regions (moisture-limited). Zscheischler et al. (2015)
 306 state that under dry conditions, evapotranspiration and temperature are strongly dom-
 307 inated by soil moisture. Especially the Mediterranean regions, the lower course of the
 308 Danube and coastal regions of the Black Sea experience $BR > 10$. Under these condi-
 309 tions, a reduced latent heat flux (and hence evaporation) suggests low soil moisture avail-
 310 ability, while temperatures rise (Mukherjee et al., 2023). Consequently, cloud convec-
 311 tion and precipitation are inhibited.

312 We find no BR inversions or only small increases during CDHE in Northern and
 313 central Europe as well as in mountainous regions (fig. 2 (a)–(b)). However, these regions
 314 are characterized by evaporation increases (and hence soil drying) during CDHE sum-
 315 mers (fig. 2 (c)). This suggests an increase in latent heat flux and, potentially, a reduced
 316 temperature increase due to evaporative cooling (O et al., 2022). These regions are char-
 317 acterized by an energy-limited evapotranspiration regime (Teuling et al., 2009), where
 318 higher temperatures in CDHE summers compared to non-CDHE summers favor evap-
 319 oration. The remainder of the domain, largely defined by soil-moisture limited evapo-
 320 transpiration regimes (Teuling et al., 2009), experiences major evaporation reductions
 321 (fig. 2 (c)), presumably due to moisture limitations in comparison to non-CDHE sum-
 322 mers. High BR values, i.e., low latent heat flux compared to sensible heat flux, may re-
 323 sult from low soil moisture conditions (Trenberth & Shea, 2005). Since soil moisture and
 324 evaporation mutually influence each other and CDHE affect evaporation (Miralles et al.,
 325 2019), we conclude here that soil moisture is affected by CDHE occurrences as well.

326 The described relationships for CDHE and non-CDHE hold true for GWL2 and
 327 GWL3 (see supplementary fig. S2 for BR evolution under GWL2 and GWL3).

328 3.2 CDHE Frequency Increases

329 CDHE occur rarely under current climate conditions (fig. 3 (a)). Assuming no de-
 330 pendence between temperature and precipitation, the occurrence probability of a CDHE
 331 would amount to $0.05 \times 0.05 = 0.0025 = 0.25$ events per 100 years. This corresponds
 332 to a 1-in-400 year event. This very rare frequency is however exceeded over most of Eu-
 333 rope. Assuming total dependence, the frequency has an upper limit at 5 events per 100
 334 years by definition of the CDHE events, equaling a 1-in-20 year event. In the CRCM5-

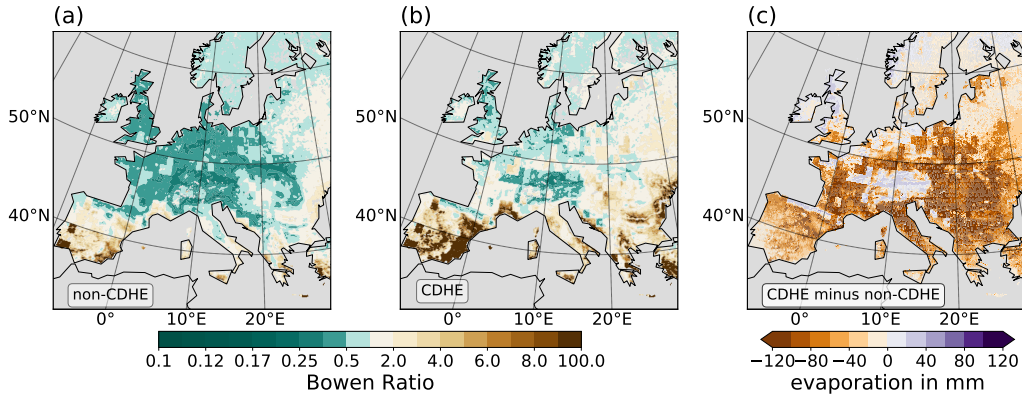


Figure 2. Bowen Ratio for non-CDHE summers (a) and CDHE summers (b) under current climate conditions. The median across all ensemble members is shown per category. Brownish colors indicate regions with sensible heat > latent heat, greenish colors indicate regions with sensible heat < latent heat. (c) evaporation increases (purple) and decreases (orange) in CDHE summers compared to non-CDHE summers under current conditions.

335 LE, highest event frequencies reach 3.5 events per 100 years in central eastern Europe
 336 (roughly 1-in-28 year event). On the contrary, parts of the Mediterranean, Aegean and
 337 Black Sea coastal regions as well as Southern Ireland, Northern France, and mountain-
 338 ous regions in central and Northern Europe encounter < 0.5 events per 100 years which
 339 corresponds to a 1-in-200 year event.

340 For GWL2, event frequencies regionally double to triple, with strongest increases
 341 in Southern Europe and weakest changes in Northern and central eastern Europe as well
 342 as the Western Iberian Peninsula (fig. 3 (b)). No decreases are detected. Interestingly,
 343 while some regions with highest event frequencies under current conditions, e.g., central
 344 eastern Europe, encounter only increases by < 3 events per 100 years, Southeastern France
 345 both shows high frequencies under current conditions and strong increases under GWL2.
 346 Contrasting to that, the coastal areas of the Mediterranean, Aegean and Black Sea with
 347 low event occurrences under current conditions experience an even higher increase by
 348 6–9 events per 100 years.

349 With further ascending GWL, event frequencies surge (fig. 3 (c)): Especially in moun-
 350 tainous forelands of Northern/Northeastern Spain and central/Southwestern France more
 351 than 1 out of 4 years under GWL3 qualify as a CDHE with respect to current percentile
 352 definitions (adding frequencies in fig. 3 (a) and (c)). The same holds true for the Po Val-
 353 ley in Northern Italy. Regions north of the Alps, in Northern France, Southern Ireland
 354 or the Western Iberian Peninsula with currently very few events (< 0.5 per 100 years)
 355 experience up to > 15 events per 100 years in addition to current frequencies. East-
 356 ern Europe and the Balkans are characterized by a North–South gradient of increases.
 357 Lowest gains are found in Scandinavia, Northeastern Europe, the highest Alpine ridges,
 358 and Southern Spain. To put these numbers into perspective, Toreti et al. (2019) show
 359 that 2018-like droughts mirror typical summer conditions by the 2040s, using a multi-
 360 model ensemble under RCP8.5.

361 3.3 Drivers of CDHE Frequency Increases

362 What is driving these frequency increases? In fig. 4, we investigate changes in the
 363 bivariate distribution of temperature and precipitation. First, fig. 4 (a)–(b) demonstrate
 364 the prevalent dominance of temperature increases in shifting the distribution into the

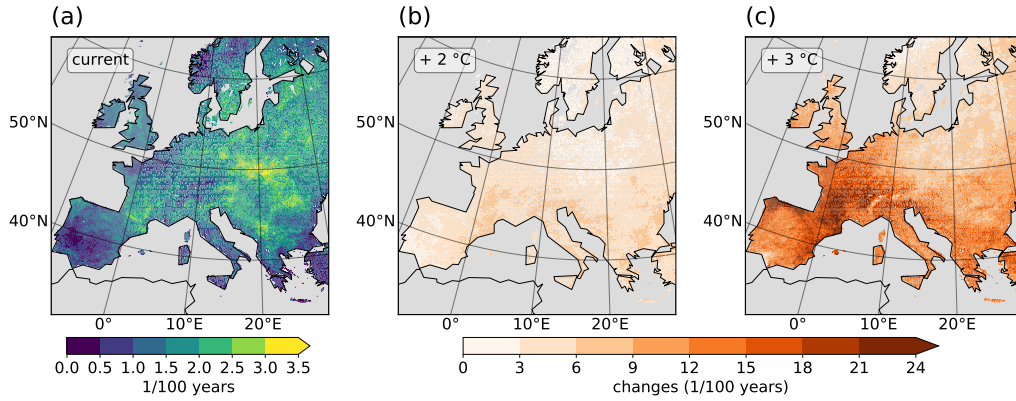


Figure 3. CDHE frequency for three global warming levels (absolute values for present climate (a) and changes under GWL2 (b) and GWL3 (c)). Events are defined as local exceedance of the current (2001–2020) 95th percentile of temperature and (negative) precipitation.

365 defined CDHE diagram space (see also fig. 1 (b)) under both GWL2 and GWL3. Pre-
 366 cipitation dominates in mountainous Norway and Northern Spain. In the Atlantic re-
 367 gions of Western Europe, temperature and precipitation changes jointly foster frequency
 368 increases. Under GWL3 conditions, these areas with mixed drivers expand towards the
 369 East. In addition, precipitation dominance emerges from previously mixed driver regions.
 370 This finding mirrors earlier emergence of (mean summer) temperature trends compared
 371 to higher uncertainty and variability in precipitation trends (e.g., von Trentini et al., 2019;
 372 Seneviratne et al., 2021). For large parts of Europe, precipitation variability defines hence
 373 whether a CDHE occurs, if (nearly) every year exceeds the present temperature thresh-
 374 old of event definition (consistent with e.g., Zscheischler & Fischer, 2020).

375 Secondly, we consider the dependence structure of the distributions (fig. 4 (c)–(e)).
 376 As stated above, a tail dependence of 1 implies that each temperature extreme (as de-
 377 fined here) is associated with a precipitation extreme and vice versa. The joint occur-
 378 rence probability of CDHE is thus 0.05 (i.e., 5 events per 100 years) and hence the same
 379 as for univariate extremes in our definition. On the contrary, a tail dependence of 0 im-
 380 plies independent behavior of temperature and precipitation extremes and thus a prob-
 381 ability of $0.05 \times 0.05 = 0.0025$ (i.e., 0.25 events per 100 years in our case). It follows
 382 that the spatial distribution in fig. 4 (c) mirrors the spatially distributed CDHE frequen-
 383 cies (fig. 3 (a)) with highest tail dependence corresponding to highest event frequencies
 384 in central eastern Europe and bivariate tail independence in mountainous Norway, North-
 385 ern France, Southern Ireland, inner Alpine regions, and Mediterranean coastal regions
 386 with very rare CDHE occurrence. Under GWL2, the tail dependence exceeds the cur-
 387 rent 95 % confidence interval especially in regions with currently low tail dependence val-
 388 ues (e.g., Northeastern France and Northern Italy, the Danube delta or mountainous Nor-
 389 way, fig. 4 (d)). In these regions, the tail dependence increase may add to event frequency.
 390 Tail dependence reductions are found on the western Iberian Peninsula with already low
 391 values and, notably, in central eastern Europe with currently highest values. More spa-
 392 tially distinct clusters emerge under GWL3 (fig. 4 (e)), where robust tail dependence in-
 393 creases occur in Northern France, Southern UK and Ireland, the Alpine (foreland) and
 394 Cantabrian Mountain regions, and Scandinavia. Tail dependence decreases, e.g., in South-
 395 ern Sweden, parts of the Iberian Peninsula, and central eastern Europe. In South-western
 396 Spain, this decrease may contribute to the rather low CDHE occurrence increase under
 397 GWL3 conditions (see fig. 3 (c)). Tail dependence changes are reflected by changes in
 398 the underlying copula family (supplementary fig. S3 (a)–(c)): For example, tail depen-

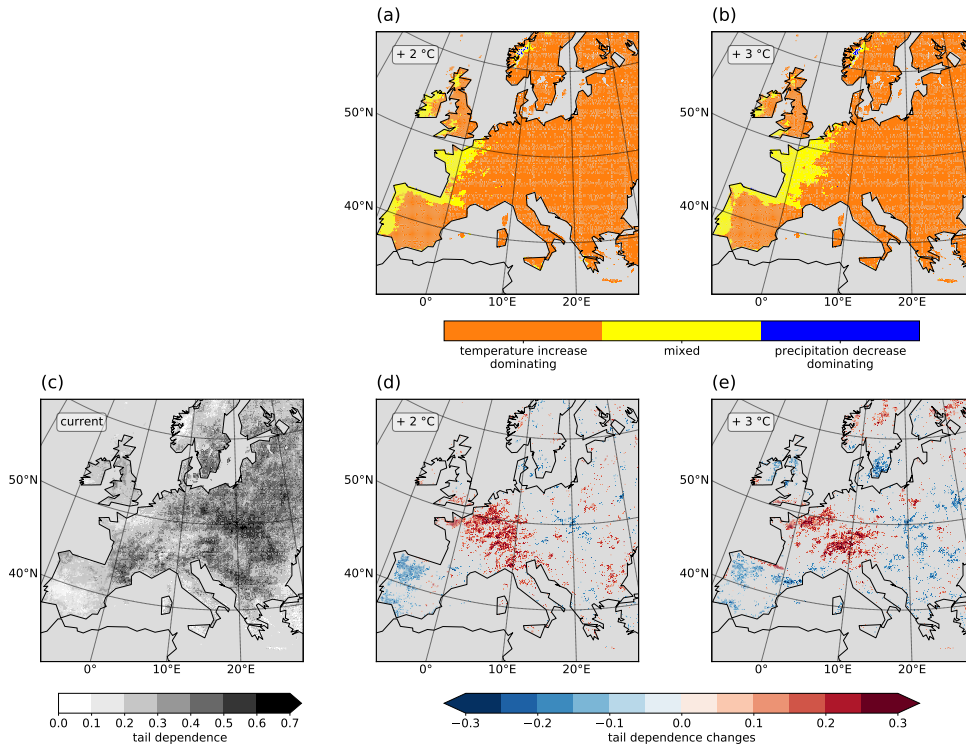


Figure 4. Changes in combined temperature and precipitation distributions. (a)–(b) distributional shifts due to temperature increases (orange), precipitation decreases (blue) or both (yellow) following the approach from fig. 1 (b)). Only land areas with significant correlations of JJA temperature and precipitation are colored. (c)–(e) tail dependence of temperature and (negative) precipitation: (c) current absolute values, changes for GWL2 (d) and GWL3 (e). For GWL2 and GWL3 only regions with changes exceeding the present 95 % confidence interval are shown. Note: The tail dependence refers to the tails above the respective 95th temperature and (negative) precipitation percentile of each period.

399 dence increases mostly correspond to switches from symmetric copula families (mostly
 400 Gaussian or Frank) to asymmetric families (e.g., Gumbel which only occur in regions with
 401 $BR < 1$ under current conditions). Decreases are associated with the inverted switch.
 402 Symmetric families represent regions with amplified tail dependence in the hot-dry and
 403 cold-wet tail, whereas asymmetric families include only one tail with enhanced depen-
 404 dence. Note that the bivariate structure is generally weak to moderate in most regions
 405 (theoretical Kendall's τ with $0.2 < \tau < 0.5$, fig. S2 (d)–(f)), pointing towards rather
 406 similar bivariate distributions. With increasing GWL, τ increases in Western Europe,
 407 hence strengthening the differences between the joint summer temperature–precipitation
 408 distributions.

409 The tail dependence also allows for a quick change of perspective: Since it is cal-
 410 culated with respect to each period (current, GWL2, GWL3), we are also able to infer
 411 that CDHEs defined relative to the percentiles of each period occur more (less) frequently
 412 where tail dependence increases (decreases).

413 3.4 Soil Moisture Scaling with CDHE Extremeness

414 To account for the risk that agricultural droughts, i.e., soil moisture deficits, pose
 415 on crops, we focus our further assessment on European agricultural regions.

416 We start our assessment with return periods T of CDHE in current, GWL2, and
 417 GWL3 conditions (fig. 5 (a)–(c)). Therefore, we ask the question: How extreme would
 418 a future CDHE be in relation to the current temperature and precipitation distribution?
 419 Since higher return periods correspond to hotter and drier summers with respect to cur-
 420 rent CDHE, they are interpreted as surrogates for joint event intensity. T is obtained
 421 for the 95th percentile of temperature and (negative) precipitation of the respective pe-
 422 riods from the copula fitted to the present bivariate distribution. Hence under current
 423 conditions (fig. 5 (a)), the distribution again mirrors the current tail dependence (fig. 4 (c))
 424 and event frequency distribution (fig. 3 (a)). The theoretical minimum return period of
 425 the current period is $T = 20$ (perfect tail dependence), the maximum $T = 400$ (inde-
 426 pendence). Consistent with that, we find among the CDHE just passing both thresh-
 427 olds return periods of $T = 30$ to $T = 300$ in the current period. Under GWL2 condi-
 428 tions (fig. 5 (b)), return periods increase to several hundreds to thousands of years with
 429 respect to the current distribution. In single grid cells (dark red), the extremeness of these
 430 CDHE is unprecedented ($T = \text{inf.}$). In these cases, (mostly) future temperature or pre-
 431 cipitation lie outside the margins of the current distribution. Hence CDHE of this ex-
 432 tremeness did not occur at all in the current period of the CRCM5-LE. Under GWL3
 433 (fig. 5 (c)), these CDHE are dominating across Europe: We find $T = 1000$ to $T = 3000$
 434 years in eastern Germany, Poland, and the Baltics, whereas the remainder of Europe is
 435 subject to CDHE with a current occurrence probability $p = 0$. To generalize, the con-
 436 ditions of CDHE definition correspond to highly unlikely current conditions when con-
 437 sidering GWL2, and unprecedented conditions in GWL3.

438 During all summers exceeding the respective CDHE definition in current, GWL2,
 439 and GWL3 climates (fig. 5 (d)–(f)), extreme (below 5th percentile) or exceptional droughts
 440 (below 2nd percentile) prevail in European agricultural regions. Exceptions are very southerly
 441 parts (Southern Spain, Turkey) where the soil moisture content corresponds to moder-
 442 ate (below 20th percentile) or severe (below 10th percentile) droughts. However, since
 443 SMI classes are calculated with respect to the local distribution and the local distribu-
 444 tions do not always range from total depletion to total saturation, the ‘less severe’ cat-
 445 egories may represent low absolute soil moisture conditions as well, while more severe
 446 drought conditions in humid regions may represent higher absolute soil moisture con-
 447 ditions. With rising GWL, virtually all European agricultural areas experience excep-
 448 tional drought conditions during future CDHE.

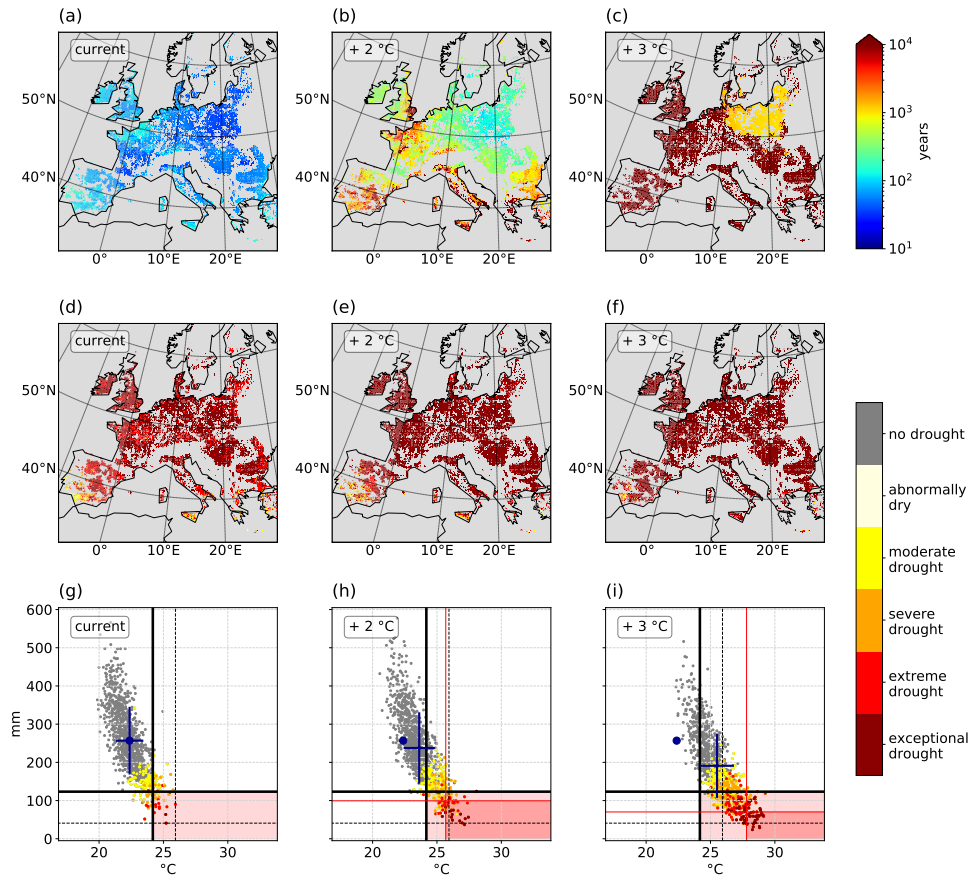


Figure 5. CDHE intensity for current, GWL2 and GWL3 conditions in European agricultural regions. (a)–(c) return period of summers with temperatures and (negative) precipitation at the GWL-specific 95th percentile (crosses of thick black lines in (g) and red lines in (h) and (i)). (d)–(f) average SMI categories during all summers exceeding the GWL-specific 95th percentiles of temperature and (negative) precipitation. (g)–(i) scatter plots of summer precipitation against summer temperature for an example region (Po Valley, Northern Italy). Thick (thin) black lines show the present 5th and 95th percentiles (minimum and maximum) for precipitation and temperature, respectively. Red lines mark the 5th and 95th percentiles for GWL2 and GWL3. Light red background highlights current CDHE summers; strong red background CDHE summers for GWL2 and GWL3 percentiles. Blue dots show the current mean, crosses span one standard deviation of the respective periods for temperature and precipitation. Colors in (d)–(i) indicate soil moisture drought categories (percentiles) with respect to the current period following Zink et al. (2016).

449 Figures 5 (g)–(i) further show the relationship among soil moisture droughts and
 450 compound events in an example region (Po Valley, south of the Alps) to illustrate the
 451 relationship between temperature, precipitation and SMI in all summers: Summers within
 452 the shaded diagram space (i.e., CDHE) are affected by more extreme SMI categories in
 453 all periods; under GWL3 the majority of CDHE summers corresponds to ‘exceptional
 454 drought’ (fig. 5 (i)). Soil moisture drought extremeness follows the distributional axis,
 455 (i.e., not dominantly along the temperature or precipitation axis). With progressing global
 456 climate change, distribution shifts towards warmer and drier conditions (see crosses re-
 457 lative to blue dots in (h) and (i)) increase the frequency of summers within the light red
 458 shaded diagram space and also more extreme SMI. The majority of CDHE summers in
 459 GWL2 and GWL3 is characterized by unprecedented temperatures (dotted black ver-
 460 tical line) and numerous future events undercut the driest current summer as well (dot-
 461 ted black horizontal line). This fact illustrates why this region is colored in dark red in
 462 fig. 5(c). CDHE frequencies even increase with respect to the future percentiles (dark
 463 red shaded diagram space) which aligns with risen tail dependence in this region (fig. 4 (h)–
 464 (i)). Overall, figs. 5 (g)–(i) suggest a stable relationship of high (low) absolute temper-
 465 ature (precipitation) values and soil moisture drought categories.

466 Last, how is bivariate extremeness of summers related to SMI? Figures 6 (a)–(c)
 467 provide Spearman rank correlations well below -0.8 in most of European agricultural ar-
 468 eas. This strong relationship implies that more extreme CDHE translate to lower mois-
 469 ture conditions. Note that the correlation does not allow to conclude whether CDHE are
 470 triggered or enhanced by low SMI values or vice versa, e.g., via land-atmosphere feed-
 471 backs. As discussed in Manning et al. (2019) and Mukherjee et al. (2023), both is plau-
 472 sible and most likely interconnected. In addition, soil moisture effects from previous sea-
 473 sons or years (Felsche et al., 2023; Bastos et al., 2020) may confound the effect of CDHE
 474 on soil moisture conditions of the same summer. The correlation is highly linear in all
 475 GWLs (fig. 6 (d)–(f)), with a shift from low event extremeness and high soil moisture
 476 in the example region during current conditions to high event extremeness and low soil
 477 moisture conditions under GWL3. Again, this mirrors large projected CDHE frequency
 478 increases both in absolute terms and relative to all summers of a given GWL epoch. These
 479 summers hence pose a triple hazard to ecosystems and agriculture in the affected regions,
 480 arising from low soil moisture, high temperature and thus high water demand for trans-
 481 piration, and low precipitation.

482 4 Discussion

483 In this study, we assessed frequency increases of European CDHE within a regional
 484 SMILE, drivers of these increases, and the association of CDHE with soil moisture droughts.
 485 The study does not provide insights in the causal directions of the SMI–CDHE relation-
 486 ship, i.e., answer the question whether low soil moisture results in or from CDHE occur-
 487 rence.

488 Defining CDHE based on summer precipitation percentiles comes at a cost as we
 489 found in our results: In very dry regions, precipitation fluctuates on a low level. Hence,
 490 due to the local JJA precipitation distribution, absolute differences between years be-
 491 low or above the percentile threshold are rather small. Here, temperature variability de-
 492 fines whether a CDHE occurs during a given period. Note that this is a different effect
 493 than precipitation variability driving CDHE occurrence in areas where regional warm-
 494 ing induces yearly exceedance of the temperature threshold. Compared to the remain-
 495 der of the domain, lag effects may play a more important role in soil moisture contents
 496 in areas with very low JJA precipitation sums. In general, CDHE may be more precisely
 497 defined with a Survival Kendall hazard definition instead of the AND definition (see, e.g.,
 498 in fig. 5 (g)–(i), Salvadori et al., 2016). However, the correlation of SMI and CDHE ex-
 499 tremeness is highly linear even in our simplified event definition.

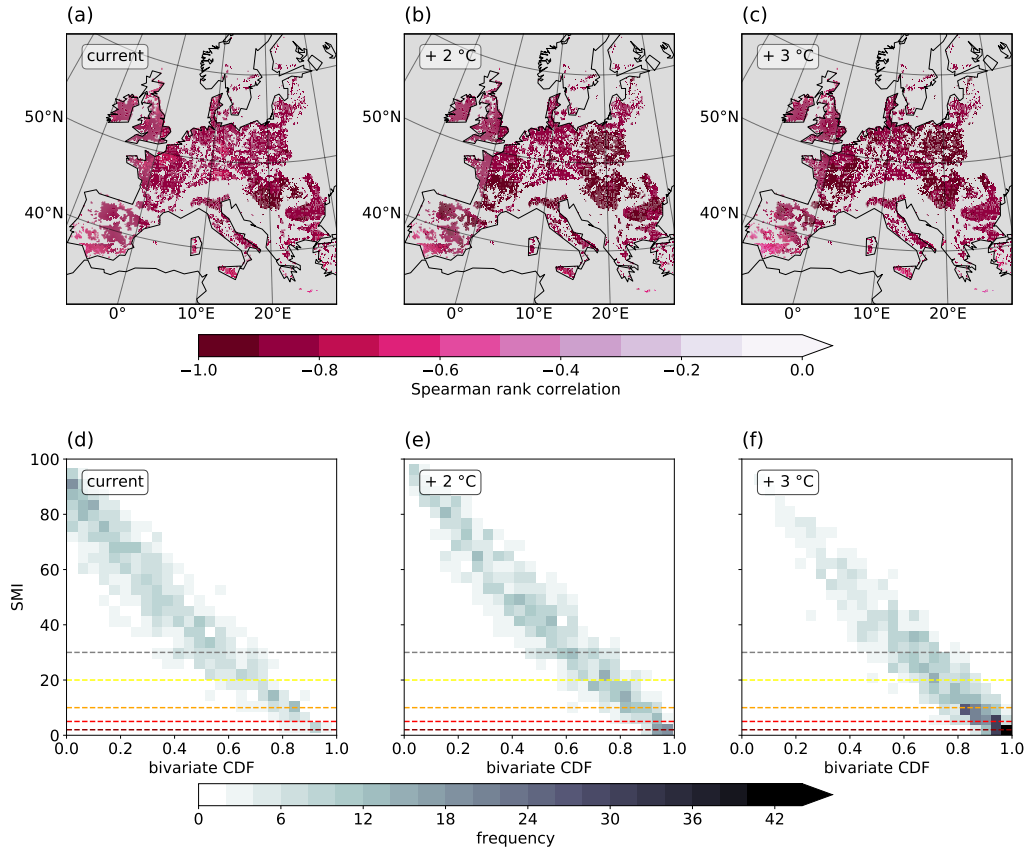


Figure 6. Relationship between CDHE extremeness (relative to conditions of the current period) and SMI values. (a)–(c) Spatially distributed Spearman rank correlation of CDHE extremeness and SMI values. (d)–(f) bivariate histograms of spatially aggregated CDHE extremeness and SMI in an example region (Po Valley, Northern Italy). Colors indicate the amount of summers in a given square. Dashed lines correspond to abnormally dry (grey), moderate drought (yellow), severe drought (orange), extreme drought (red), and exceptional drought (dark red) SMI conditions expressed as percentiles following Zink et al. (2016).

500 For explaining CDHE frequency increases, we focused on temperature and precip-
 501 itation mean shifts, i.e., no variability or higher-order distributional changes which are
 502 represented, e.g., in the marginal changes in François and Vrac (2023). Inspections of
 503 local distributions showed that for summer CDHE variability changes only marginally
 504 under GWL2 and GWL3 (e.g., fig. 5 (d)–(f)). Shifts of the joint distributions alone were
 505 shown to considerably increase CDHE frequencies – not only in arid regions as done by
 506 Hao et al. (2018) and Mukherjee and Mishra (2021), but also in transitional/humid re-
 507 gions. Our approach is limited by the margins of the current temperature and precip-
 508 itation distributions since we relate future events to the current distribution. Neverthe-
 509 less, we showed that the joint increase of hot and dry extremeness can be used as a qual-
 510 itative intensity measure. Beyond that, Wang et al. (2021) pointed to regionally inten-
 511 sifying negative correlations between temperature and precipitation over the last decades
 512 which led to an increase of CDHE, especially in the form of more heat events during droughts.
 513 However, we show that not only correlation of the full distribution is projected to change
 514 with rising GWL, but also the distributional tails and the entire dependence structure.
 515 Bivariate dependence structures in models though require cautious consideration. Zscheischler
 516 and Fischer (2020) point towards an underestimation of temperature and precipitation
 517 tail dependence in CMIP5 models. This would imply a potential underestimation of CDHE.
 518 A more detailed investigation into bivariate distributional characteristics in model and
 519 observational data is hence advisable for locally specific assessments.

520 By reaching GWL3 in the middle of the 21st century (2042–2061) under RCP8.5,
 521 the CanESM2 driving the CRCM5-LE proves to be a rather hot global climate model.
 522 We therefore used a relative model- and scenario-independent measure of time, i.e., the
 523 GWL, to overcome the effect of an intrinsically ‘hot’ global climate model with a high-
 524 emission scenario. Assessing uncertainties related to this approach requires comparative
 525 studies in other model SMILEs and with other scenarios. Yet, so far, there is only a very
 526 limited number of regional SMILEs (typically with only few members) available (e.g.,
 527 Aalbers et al., 2018).

528 As argued in Jha et al. (2023), the selection of warming levels and models explains
 529 most of the uncertainty in CDHE changes over Europe. The choice of copula families
 530 contributes the least in their assessment, while Zscheischler and Fischer (2020) argue that
 531 event definition and copula fitting affect the final probability and therefore extremeness
 532 of events. In our study, we attempted to reduce this kind of uncertainty by not focus-
 533 ing on single events. Instead, the SMILE served as a basis for investigating general char-
 534 acteristics of a large number of events, thus reducing the influence of outliers. Testing
 535 several copula families helped to find the locally best fitting bivariate distribution. Fur-
 536 ther, while in principle the SMILE provides the required size to sample low-probability
 537 events ($T = 1000$), we found that future events tend to be clearly more rare than cur-
 538 rent 1-in-1000 year events. Hence, even the large ensemble is insufficient for empirical
 539 estimations and distributional sampling is necessary.

540 Using the SMILE though allows for a robust sampling of internal variability which
 541 potentially masks dependence changes in setups with few members (Bevacqua et al., 2023).
 542 In addition, differing states of large-scale atmospheric modes prevalent in single mem-
 543 bers during the selected period of investigation may trigger differences in compound event
 544 frequencies (Bevacqua et al., 2023). This shows the high importance of internal variabil-
 545 ity in the evaluation of low-probability events and justifies the use of a SMILE.

546 While the CRCM5-LE provides high geographical detail in the spatial distribution
 547 of frequency (changes), results are affected by coarse resolution geophysical inputs as is
 548 visible in fig. 2: The tiling pattern resolution (1°) is coarser than the CRCM5 resolution,
 549 but finer than the spatial resolution of the driving general circulation model CanESM2.
 550 In central Europe, high bedrock depths (i.e., large soil column) coincide particularly well
 551 with low BR in fig. 2 (b) and high evaporation in fig. 2 (c). Presumably, a large soil col-
 552 umn contributes more strongly to evaporation than neighboring areas with thin soil columns.

553 However, this assumption requires further investigation, as well as implications on the
 554 reliability of other variables. For instance, this effect is also visible in the upper distri-
 555 butional tail of temperature at high temporal resolution (see also Miller et al., 2023). In
 556 spite of this, the regional SMILE allowed to highlight hotspots of event frequency (changes)
 557 and regionally varying driver dominance in high geographical detail. This is a large ad-
 558 vantage of our study over similar analyses with coarse-resolution global SMILEs: For ex-
 559 ample, a distinction of coastal or mountainous regions would not be possible on a coarse
 560 grid since the small-scale features cannot be resolved. Hence, the derivation of relevant
 561 drivers or dependence changes would have been impeded.

562 Given considerable frequency increases of CDHE and their association to low soil
 563 moisture contents, we argue that the relationship between both deserves further inves-
 564 tigation. Denissen et al. (2022) show that soil moisture limited conditions represent the
 565 new normal under a high-emission global warming scenario in that they intensify and
 566 expand in length. Since it has been shown that heatwaves, droughts or compound CDHE
 567 can be triggered by depleted soils (Fischer et al., 2007), investigating CDHE effects on
 568 soil moisture is also crucial in bringing forth the research on potential legacy effects on
 569 subsequent seasons or years (e.g., CDHE triggering subsequent CDHE mediated by pre-
 570 vailing soil depletion). CDHE may exert influence not only on temporally, but also spa-
 571 tially distant events: Li et al. (2023) show that dry soils in upwind regions may lead to
 572 propagation of events and, adding onto local land-atmosphere coupling, affect crop yields
 573 downwind of events. For example, these authors found that maize failure in Southeast-
 574 ern Europe and wheat failure in Italy tend to be associated with dry and hot conditions.

575 5 Conclusions

576 We find that European compound hot and dry summers are characterized by an
 577 increase of evaporative demand in the atmosphere, but with reduced evaporation in most
 578 regions, presumably due to soil moisture deficits. Mountainous regions experience increased
 579 evaporation, most likely due to higher temperatures and still dominant energy limita-
 580 tion of their evaporation regime. The frequency of CDHE summers increases consider-
 581 ably in Europe under climate change conditions. Owing to the high spatial resolution
 582 of our SMILE, we robustly identify regions in Southern France and Northern Spain as
 583 hotspots due to highest absolute increases, whereas, e.g., Southern Germany, Northern
 584 France, Southern Ireland, or the southwestern Black Sea coast can be identified as cur-
 585 rently low-frequency areas with highest multiplication of events under climate change.
 586 Apart from Western European regions, Northern Spain and mountainous Norway, fre-
 587 quency increases can be mostly attributed to rising temperatures. Yet, climate change
 588 also affects the bivariate dependence structure of temperature and precipitation, foster-
 589 ing tail dependencies and hence the co-occurrence of dry and hot conditions. Further,
 590 events intensify with respect to the current conditions of precipitation and temperature.
 591 Soil moisture during CDHE is projected to remain extremely low under GWL2 and GWL3
 592 in agricultural regions and shows particularly strong negative correlations with bivari-
 593 ate summer intensity.

594 This study finds newly emerging CDHE hotspots in European areas with yet un-
 595 seen combinations of extremely hot and dry conditions. Regardless of the causal direc-
 596 tions in the SMI-CDHE relationship, the tight relationship of low soil moisture and CDHE
 597 therefore poses an increasing risk to agriculture that requires consideration in adapta-
 598 tion planning.

599 This study also shows an ordering of temperature and precipitation changes in driv-
 600 ing the frequency increases: For GWL2, temperature increase is the major driver of CDHE
 601 frequency increases. For GWL3, precipitation decrease additionally emerge as impor-
 602 tant driver (in the form of mixed contributions). Here, it would be interesting to further
 603 investigate the processes and mechanisms driving local dependence increases or decreases.

604 The regional SMILE is particularly apt for analyzing compound events in the ex-
 605 tremite tails of the bivariate distribution. Climate change is shown to produce events that
 606 are much rarer than any observed summer, while currently extremely rare events become
 607 the new normal. Fitting distributions instead of counting the summers that meet the
 608 event definition criteria hence allows to avoid a saturation effect related to the maximum
 609 empirical event rareness under current conditions (i.e., $T = 1000$ years). Using SMILEs,
 610 further research can elucidate potential benefits of increasing sample sizes in reducing
 611 the uncertainty ranges of distribution fitting for extremely rare events.

612 Last, we conclude that limiting global warming to +2 °C considerably reduces CDHE
 613 hazards in Europe, which regionally then results in half the amount of summers with ex-
 614 tremely low soil moisture availability. Since the risk of impacts on human systems de-
 615 pends on resilience structures in the affected regions (e.g., Lesk et al., 2016), hazard re-
 616 duction should be accompanied by fostering resilience towards CDHE effects as well.

617 Open Research Section

618 The CRCM5-LE data used for all performed analyses is described in Leduc et al.
 619 (2019) and available at <https://www.climex-project.org/en/data-access/>

620 Corine land cover data is provided by the European Union, Copernicus Land Mon-
 621 itoring Service 2018, European Environment Agency (EEA) at [https://land.copernicus.eu/pan-](https://land.copernicus.eu/pan-european/corine-land-cover)
 622 [european/corine-land-cover](https://land.copernicus.eu/pan-european/corine-land-cover)

623 Codes to perform the presented analyses and obtain the figures will be shared through
 624 a public repository upon publication of the manuscript.

625 Acknowledgments

626 This research was conducted within the ClimEx project (www.climex-project.org) funded
 627 by the Bavarian State Ministry for the Environment and Consumer Protection (Grant
 628 No. 81-0270-024570/2015). CRCM5 was developed by the ESCER Centre of Université
 629 du Québec à Montréal (UQAM; <https://escer.uqam.ca/>, last access: 14 June 2023) in
 630 collaboration with Environment and Climate Change Canada. Computations with the
 631 CRCM5 for the ClimEx project were performed on the HPC system SuperMUC and the
 632 Linux Cluster of the Leibniz Supercomputing Center LRZ, Bavarian Academy of Sci-
 633 ences and the Humanities (BAdW), funded via GCS by BMBF and StMWFK. The au-
 634 thors gratefully acknowledge the Leibniz Supercomputing center for funding this project
 635 by providing computing time on its Linux-Cluster. Further, the authors would like to
 636 thank H. Funk for fruitful discussions on copula use.

637 References

- 638 Aalbers, E. E., Lenderink, G., van Meijgaard, E., & van den Hurk, B. J. J. M.
 639 (2018). Local-scale changes in mean and heavy precipitation in western eu-
 640 rope, climate change or internal variability? *Climate Dynamics*, *50*, 4745-
 641 4766. Retrieved from <https://doi.org/10.1007/s00382-017-3901-9> doi:
 642 10.1007/s00382-017-3901-9
- 643 Afroz, M., Chen, G., & Anandhi, A. (2023). Drought- and heatwave-associated com-
 644 pound extremes: A review of hotspots, variables, parameters, drivers, impacts,
 645 and analysis frameworks. *Frontiers in Earth Science*, *10*. Retrieved from
 646 <https://www.frontiersin.org/articles/10.3389/feart.2022.914437>
 647 doi: 10.3389/feart.2022.914437
- 648 AghaKouchak, A., Cheng, L., Mazdidasni, O., & Farahmand, A. (2014). Global
 649 warming and changes in risk of concurrent climate extremes: Insights from
 650 the 2014 california drought. *Geophysical Research Letters*, *41*(24), 8847-8852.
 651 Retrieved from <https://agupubs.onlinelibrary.wiley.com/doi/abs/>

- 652 10.1002/2014GL062308 doi: <https://doi.org/10.1002/2014GL062308>
- 653 Bastos, A., Ciais, P., Friedlingstein, P., Sitch, S., Pongratz, J., Fan, L., ... Zaehle, S.
654 (2020). Direct and seasonal legacy effects of the 2018 heat wave and drought
655 on european ecosystem productivity. *Science Advances*, 6(24), eaba2724. Re-
656 trieved from <https://www.science.org/doi/abs/10.1126/sciadv.aba2724>
657 doi: 10.1126/sciadv.aba2724
- 658 Bevacqua, E., Maraun, D., Hobæk Haff, I., Widmann, M., & Vrac, M. (2017). Multi-
659 variate statistical modelling of compound events via pair-copula constructions:
660 analysis of floods in ravenna (italy). *Hydrology and Earth System Sciences*,
661 21(6), 2701–2723. Retrieved from [https://hess.copernicus.org/articles/](https://hess.copernicus.org/articles/21/2701/2017/)
662 [21/2701/2017/](https://hess.copernicus.org/articles/21/2701/2017/) doi: 10.5194/hess-21-2701-2017
- 663 Bevacqua, E., Suarez-Gutierrez, L., Jézéquel, A., Lehner, F., Vrac, M., Yiou, P., &
664 Zscheischler, J. (2023). Advancing research on compound weather and climate
665 events via large ensemble model simulations. *Nature Communications*, 14,
666 2145. Retrieved from <https://doi.org/10.1038/s41467-023-37847-5> doi:
667 10.1038/s41467-023-37847-5
- 668 Bowen, I. S. (1926). The ratio of heat losses by conduction and by evaporation from
669 any water surface. *Physical Review*, 27, 779-787.
- 670 Brunner, M. I., Seibert, J., & Favre, A.-C. (2016). Bivariate return periods and their
671 importance for flood peak and volume estimation. *WIREs Water*, 3(6), 819-
672 833. Retrieved from [https://wires.onlinelibrary.wiley.com/doi/abs/10](https://wires.onlinelibrary.wiley.com/doi/abs/10.1002/wat2.1173)
673 [.1002/wat2.1173](https://wires.onlinelibrary.wiley.com/doi/abs/10.1002/wat2.1173) doi: <https://doi.org/10.1002/wat2.1173>
- 674 Buras, A., Rammig, A., & Zang, C. S. (2020). Quantifying impacts of the 2018
675 drought on european ecosystems in comparison to 2003. *Biogeosciences*, 17(6),
676 1655–1672. Retrieved from [https://bg.copernicus.org/articles/17/1655/](https://bg.copernicus.org/articles/17/1655/2020/)
677 [2020/](https://bg.copernicus.org/articles/17/1655/2020/) doi: 10.5194/bg-17-1655-2020
- 678 Böhnisch, A., Felsche, E., & Ludwig, R. (2023). European heatwave tracks: using
679 causal discovery to detect recurring pathways in a single-regional climate
680 model large ensemble. *Environmental Research Letters*, 18(1), 014038.
681 Retrieved from <https://dx.doi.org/10.1088/1748-9326/aca9e3> doi:
682 10.1088/1748-9326/aca9e3
- 683 Böhnisch, A., Mittermeier, M., Leduc, M., & Ludwig, R. (2021). Hot spots and
684 climate trends of meteorological droughts in europe—assessing the percent of
685 normal index in a single-model initial-condition large ensemble. *Frontiers*
686 *in Water*, 3. Retrieved from [https://www.frontiersin.org/articles/](https://www.frontiersin.org/articles/10.3389/frwa.2021.716621)
687 [10.3389/frwa.2021.716621](https://www.frontiersin.org/articles/10.3389/frwa.2021.716621) doi: 10.3389/frwa.2021.716621
- 688 Ciais, P., Reichstein, N., M. and Viovy, Granier, A., Ogée, J., Allard, V., Aubinet,
689 M., ... Valentini, R. (2005). Europe-wide reduction in primary productivity
690 caused by the heat and drought in 2003. *Nature*, 437, 529–533. Retrieved from
691 <https://doi.org/10.1038/nature03972> doi: 10.1038/nature03972
- 692 Coles, S. (2001). *An introduction to statistical modeling of extreme values*. Springer
693 London.
- 694 Coles, S., Heffernan, J., & Tawn, J. (1999). Dependence measures for extreme value
695 analyses. *Extremes*, 2, 339–365. Retrieved from [https://doi.org/10.1023/](https://doi.org/10.1023/A:1009963131610)
696 [A:1009963131610](https://doi.org/10.1023/A:1009963131610) doi: 10.1023/A:1009963131610
- 697 Denissen, J. M. C., Teuling, A. J., Pitman, A. J., Koirala, S., Migliavacca, M.,
698 Li, W., ... Orth, R. (2022). Widespread shift from ecosystem energy to
699 water limitation with climate change. *Nature Climate Change*, 12, 677–
700 684. Retrieved from <https://doi.org/10.1038/s41558-022-01403-8> doi:
701 10.1038/s41558-022-01403-8
- 702 EEA, E. E. A. (2020). *Corine land cover (clc) 2018, version*
703 *2020_20u1*. ([https://land.copernicus.eu/pan-european/corine-land-](https://land.copernicus.eu/pan-european/corine-land-cover/clc2018?tab=metadata)
704 [cover/clc2018?tab=metadata](https://land.copernicus.eu/pan-european/corine-land-cover/clc2018?tab=metadata). Last accessed: 9 June 2023)
- 705 Felsche, E., Böhnisch, A., & Ludwig, R. (2023). Inter-seasonal connection of typi-
706 cal european heatwave patterns to soil moisture. *npj Climate and Atmospheric*

- 707 *Science*, 6(1), 1. doi: <https://doi.org/10.1038/s41612-023-00330-5>
- 708 Fischer, E. M., Seneviratne, S. I., Lüthi, D., & Schär, C. (2007). Contribution of
709 land-atmosphere coupling to recent european summer heat waves. *Geophysical*
710 *Research Letters*, 34(6). Retrieved from [https://agupubs.onlinelibrary](https://agupubs.onlinelibrary.wiley.com/doi/abs/10.1029/2006GL029068)
711 [.wiley.com/doi/abs/10.1029/2006GL029068](https://agupubs.onlinelibrary.wiley.com/doi/abs/10.1029/2006GL029068) doi: [https://doi.org/10.1029/](https://doi.org/10.1029/2006GL029068)
712 [2006GL029068](https://doi.org/10.1029/2006GL029068)
- 713 François, B., & Vrac, M. (2023). Time of emergence of compound events: contribu-
714 tion of univariate and dependence properties. *Natural Hazards and Earth Sys-*
715 *tem Sciences*, 23(1), 21–44. Retrieved from [https://nhess.copernicus.org/](https://nhess.copernicus.org/articles/23/21/2023/)
716 [articles/23/21/2023/](https://nhess.copernicus.org/articles/23/21/2023/) doi: 10.5194/nhess-23-21-2023
- 717 Fyfe, J. C., Derksen, C., Mudryk, L., Flato, G. M., Santer, B. D., Swart, N. C.,
718 ... Jiao, Y. (2017). Large near-term projected snowpack loss over the
719 western United States. *Nature Communications*, 8. Retrieved from
720 <https://doi.org/10.1038/ncomms14996> doi: 10.1038/ncomms14996
- 721 Gilleland, E. (2022). *extremes: Extreme value analysis. r package version 2.1-3*. Re-
722 trieved from <https://staff.ral.ucar.edu/ericg/extRemes/>
- 723 Gulev, S., Thorne, P., Ahn, J., Dentener, F., Domingues, C., Gerland, S., ... Vose,
724 R. (2021). Changing state of the climate system. In V. Masson-Delmotte et
725 al. (Eds.), *Climate change 2021: The physical science basis. contribution of*
726 *working group i to the sixth assessment report of the intergovernmental panel*
727 *on climate change*. Cambridge University Press, Cambridge, United Kingdom
728 and New York, NY, USA. doi: 10.1017/9781009157896.004
- 729 Hao, Z., Hao, F., Singh, V. P., & Zhang, X. (2018). Changes in the severity of
730 compound drought and hot extremes over global land areas. *Environment-*
731 *tal Research Letters*, 13(12), 124022. Retrieved from [https://dx.doi.org/](https://dx.doi.org/10.1088/1748-9326/aaee96)
732 [10.1088/1748-9326/aaee96](https://dx.doi.org/10.1088/1748-9326/aaee96) doi: 10.1088/1748-9326/aaee96
- 733 Hauser, M., Engelbrecht, F., & Fischer, E. M. (2022). *Transient global warming lev-*
734 *els for CMIP5 and CMIP6*. Zenodo. Retrieved from [https://doi.org/10](https://doi.org/10.5281/zenodo.7390473)
735 [.5281/zenodo.7390473](https://doi.org/10.5281/zenodo.7390473) doi: 10.5281/zenodo.7390473
- 736 Jha, S., Gudmundsson, L., & Seneviratne, S. I. (2023). Partitioning the uncertain-
737 ties in compound hot and dry precipitation, soil moisture, and runoff extremes
738 projections in cmip6. *Earth's Future*, 11(3), e2022EF003315. Retrieved
739 from [https://agupubs.onlinelibrary.wiley.com/doi/abs/10.1029/](https://agupubs.onlinelibrary.wiley.com/doi/abs/10.1029/2022EF003315)
740 [2022EF003315](https://agupubs.onlinelibrary.wiley.com/doi/abs/10.1029/2022EF003315) (e2022EF003315 2022EF003315) doi: [https://doi.org/10.1029/](https://doi.org/10.1029/2022EF003315)
741 [2022EF003315](https://doi.org/10.1029/2022EF003315)
- 742 Kirchmeier-Young, M. C., Zwiers, F. W., & Gillett, N. P. (2017). Attribution of
743 extreme events in arctic sea ice extent. *Journal of Climate*, 30(2), 553 - 571.
744 Retrieved from [https://journals.ametsoc.org/view/journals/clim/30/2/](https://journals.ametsoc.org/view/journals/clim/30/2/jcli-d-16-0412.1.xml)
745 [jcli-d-16-0412.1.xml](https://journals.ametsoc.org/view/journals/clim/30/2/jcli-d-16-0412.1.xml) doi: <https://doi.org/10.1175/JCLI-D-16-0412.1>
- 746 Kornhuber, K., Osprey, S., Coumou, D., Petri, S., Petoukhov, V., Rahmstorf, S., &
747 Gray, L. (2019). Extreme weather events in early summer 2018 connected by a
748 recurrent hemispheric wave-7 pattern. *Environmental Research Letters*, 14(5),
749 054002. Retrieved from <https://doi.org/10.1088/1748-9326/ab13bf> doi:
750 [10.1088/1748-9326/ab13bf](https://doi.org/10.1088/1748-9326/ab13bf)
- 751 Leduc, M., Mailhot, A., Frigon, A., Martel, J.-L., Ludwig, R., Brietzke, G. B.,
752 ... Scinocca, J. (2019). The climex project: A 50-member ensemble
753 of climate change projections at 12-km resolution over europe and north-
754 eastern north america with the canadian regional climate model (crcm5).
755 *Journal of Applied Meteorology and Climatology*, 58(4), 663–693. doi:
756 [10.1175/JAMC-D-18-0021.1](https://doi.org/10.1175/JAMC-D-18-0021.1)
- 757 Leonard, M., Westra, S., Phatak, A., Lambert, M., van den Hurk, B., McInnes, K.,
758 ... Stafford-Smith, M. (2014). A compound event framework for understand-
759 ing extreme impacts. *WIREs Climate Change*, 5(1), 113–128. Retrieved from
760 <https://wires.onlinelibrary.wiley.com/doi/abs/10.1002/wcc.252> doi:
761 <https://doi.org/10.1002/wcc.252>

- 762 Lesk, C., Rowhani, P., & Ramankutty, N. (2016). Influence of extreme weather
763 disasters on global crop production. *Nature*, *529*, 84–87. Retrieved from
764 <https://doi.org/10.1038/nature16467> doi: 10.1038/nature16467
- 765 Li, H., Keune, J., Smessaert, F., Nieto, R., Gimeno, L., & Miralles, D. G. (2023).
766 Land–atmosphere feedbacks contribute to crop failure in global rainfed
767 breadbaskets. *npj Climate and Atmospheric Science*, *6*, 51. Retrieved
768 from <https://doi.org/10.1038/s41612-023-00375-6> doi: 10.1038/
769 s41612-023-00375-6
- 770 Liu, P. R., & Raftery, A. E. (2021). Country-based rate of emissions reduc-
771 tions should increase by 80% beyond nationally determined contributions
772 to meet the 2 °c target. *Communications Earth & Environment*, *2*, 29.
773 Retrieved from <https://doi.org/10.1038/s43247-021-00097-8> doi:
774 10.1038/s43247-021-00097-8
- 775 Maher, N., Milinski, S., & Ludwig, R. (2021). Large ensemble climate model
776 simulations: introduction, overview, and future prospects for utilising multi-
777 ple types of large ensemble. *Earth System Dynamics*, *12*(2), 401–418. Re-
778 trieved from <https://esd.copernicus.org/articles/12/401/2021/> doi:
779 10.5194/esd-12-401-2021
- 780 Manning, C., Widmann, M., Bevacqua, E., Loon, A. F. V., Maraun, D., & Vrac, M.
781 (2019). Increased probability of compound long-duration dry and hot events in
782 europe during summer (1950–2013). *Environmental Research Letters*, *14*(9),
783 094006. Retrieved from <https://dx.doi.org/10.1088/1748-9326/ab23bf>
784 doi: 10.1088/1748-9326/ab23bf
- 785 Markonis, Y., Kumar, R., Hanel, M., Rakovec, O., Máca, P., & AghaKouchak, A.
786 (2021). The rise of compound warm-season droughts in europe. *Science Ad-
787 vances*, *7*(6), eabb9668. Retrieved from [https://www.science.org/doi/abs/
788 10.1126/sciadv.abb9668](https://www.science.org/doi/abs/10.1126/sciadv.abb9668) doi: 10.1126/sciadv.abb9668
- 789 Miller, J., Böhnisch, A., Ludwig, R., & Brunner, M. I. (2023). Climate change im-
790 pacts on regional fire weather in heterogeneous landscapes of central europe.
791 *Natural Hazards and Earth System Sciences Discussions*, *2023*, 1–25. Re-
792 trieved from <https://nhess.copernicus.org/preprints/nhess-2023-51/>
793 doi: 10.5194/nhess-2023-51
- 794 Miralles, D. G., Gentile, P., Seneviratne, S. I., & Teuling, A. J. (2019).
795 Land–atmospheric feedbacks during droughts and heatwaves: state of the
796 science and current challenges. *Annals of the New York Academy of Sci-
797 ences*, *1436*(1), 19–35. Retrieved from [https://nyaspubs.onlinelibrary
798 .wiley.com/doi/abs/10.1111/nyas.13912](https://nyaspubs.onlinelibrary.wiley.com/doi/abs/10.1111/nyas.13912) doi: [https://doi.org/10.1111/
799 nyas.13912](https://doi.org/10.1111/nyas.13912)
- 800 Mukherjee, S., & Mishra, A. K. (2021). Increase in compound drought and
801 heatwaves in a warming world. *Geophysical Research Letters*, *48*(1),
802 e2020GL090617. Retrieved from [https://agupubs.onlinelibrary.wiley
803 .com/doi/abs/10.1029/2020GL090617](https://agupubs.onlinelibrary.wiley.com/doi/abs/10.1029/2020GL090617) (e2020GL090617 2020GL090617) doi:
804 <https://doi.org/10.1029/2020GL090617>
- 805 Mukherjee, S., Mishra, A. K., Zscheischler, J., & Entekhabi, D. (2023). Interac-
806 tion between dry and hot extremes at a global scale using a cascade modeling
807 framework. *Nature Communications*, *14*, 277. Retrieved from [https://
808 doi.org/10.1038/s41467-022-35748-7](https://doi.org/10.1038/s41467-022-35748-7) doi: 10.1038/s41467-022-35748-7
- 809 Nagler, T., Schepsmeier, U., Stoeber, J., Brechmann, E. C., Graeler, B., Erhardt,
810 T., . . . Vatter, T. (2023). *Vinecopula: Statistical inference of vine copulas.
811 r package version 2.4.5*. Retrieved from [https://github.com/tnagler/
812 VineCopula](https://github.com/tnagler/VineCopula)
- 813 O, S., Bastos, A., Reichstein, M., Li, W., Denissen, J., Graefen, H., & Orth, R.
814 (2022). The role of climate and vegetation in regulating drought–heat ex-
815 tremes. *Journal of Climate*, *35*(17), 5677–5685. Retrieved from [https://
816 journals.ametsoc.org/view/journals/clim/35/17/JCLI-D-21-0675.1.xml](https://journals.ametsoc.org/view/journals/clim/35/17/JCLI-D-21-0675.1.xml)

- 817 doi: <https://doi.org/10.1175/JCLI-D-21-0675.1>
- 818 Poschlod, B., Zscheischler, J., Sillmann, J., Wood, R. R., & Ludwig, R. (2020). Cli-
819 mate change effects on hydrometeorological compound events over southern
820 norway. *Weather and Climate Extremes*, *28*, 100253. Retrieved from [https://](https://www.sciencedirect.com/science/article/pii/S2212094719301574)
821 www.sciencedirect.com/science/article/pii/S2212094719301574 doi:
822 <https://doi.org/10.1016/j.wace.2020.100253>
- 823 Richardson, M. I., Cowtan, K. D., Hawkins, E., & Stolpe, M. B. (2016). Rec-
824 onciled climate response estimates from climate models and the energy
825 budget of earth. *Nature Climate Change*, *6*, 931-935. Retrieved from
826 <https://doi.org/10.1038/nclimate3066> doi: 10.1038/nclimate30660
- 827 Rousi, E., Fink, A. H., Andersen, L. S., Becker, F. N., Beobide-Arsuaga, G., Breil,
828 M., ... Xoplaki, E. (2023). The extremely hot and dry 2018 summer in central
829 and northern europe from a multi-faceted weather and climate perspective.
830 *Natural Hazards and Earth System Sciences*, *23*(5), 1699–1718. Retrieved
831 from <https://nhess.copernicus.org/articles/23/1699/2023/> doi:
832 10.5194/nhess-23-1699-2023
- 833 Salvadori, G., Durante, F., De Michele, C., Bernardi, M., & Petrella, L. (2016). A
834 multivariate copula-based framework for dealing with hazard scenarios and
835 failure probabilities. *Water Resources Research*, *52*(5), 3701-3721. Retrieved
836 from [https://agupubs.onlinelibrary.wiley.com/doi/abs/10.1002/](https://agupubs.onlinelibrary.wiley.com/doi/abs/10.1002/2015WR017225)
837 [2015WR017225](https://agupubs.onlinelibrary.wiley.com/doi/abs/10.1002/2015WR017225) doi: <https://doi.org/10.1002/2015WR017225>
- 838 Schwalm, C. R., Glendon, S., & Duffy, P. B. (2020). Rcp8.5 tracks cumulative
839 co₂ emissions. *Proceedings of the National Academy of Sciences*,
840 *117*(33), 19656-19657. Retrieved from [https://www.pnas.org/doi/abs/](https://www.pnas.org/doi/abs/10.1073/pnas.2007117117)
841 [10.1073/pnas.2007117117](https://www.pnas.org/doi/abs/10.1073/pnas.2007117117) doi: 10.1073/pnas.2007117117
- 842 Schwingshackl, C., Hirschi, M., & Seneviratne, S. I. (2017). Quantifying spa-
843 tiotemporal variations of soil moisture control on surface energy balance and
844 near-surface air temperature. *Journal of Climate*, *30*(18), 7105 - 7124. Re-
845 trieved from [https://journals.ametsoc.org/view/journals/clim/30/18/](https://journals.ametsoc.org/view/journals/clim/30/18/jcli-d-16-0727.1.xml)
846 [jcli-d-16-0727.1.xml](https://journals.ametsoc.org/view/journals/clim/30/18/jcli-d-16-0727.1.xml) doi: <https://doi.org/10.1175/JCLI-D-16-0727.1>
- 847 Seneviratne, S., Zhang, X., Adnan, M., Badi, W., Dereczynski, C., Di Luca, A., ...
848 Zhou, B. (2021). Weather and climate extreme events in a changing climate.
849 In V. Masson-Delmotte et al. (Eds.), *Climate change 2021: The physical sci-*
850 *ence basis. contribution of working group i to the sixth assessment report of the*
851 *intergovernmental panel on climate change*. doi: 10.1017/9781009157896.013
- 852 Swart, N. C., Cole, J. N. S., Kharin, V. V., Lazare, M., Scinocca, J. F., Gillett,
853 N. P., ... Winter, B. (2019). The canadian earth system model version 5
854 (canesm5.0.3). *Geoscientific Model Development*, *12*(11), 4823–4873. Re-
855 trieved from <https://gmd.copernicus.org/articles/12/4823/2019/> doi:
856 10.5194/gmd-12-4823-2019
- 857 Teuling, A. J., Hirschi, M., Ohmura, A., Wild, M., Reichstein, M., Ciais, P., ...
858 Seneviratne, S. I. (2009). A regional perspective on trends in continental
859 evaporation. *Geophysical Research Letters*, *36*(2). Retrieved from [https://](https://agupubs.onlinelibrary.wiley.com/doi/abs/10.1029/2008GL036584)
860 agupubs.onlinelibrary.wiley.com/doi/abs/10.1029/2008GL036584 doi:
861 <https://doi.org/10.1029/2008GL036584>
- 862 Toreti, A., Belward, A., Perez-Dominguez, I., Naumann, G., Luterbacher, J., Cronie,
863 O., ... Zampieri, M. (2019). The exceptional 2018 european water seesaw
864 calls for action on adaptation. *Earth's Future*, *7*(6), 652-663. Retrieved
865 from [https://agupubs.onlinelibrary.wiley.com/doi/abs/10.1029/](https://agupubs.onlinelibrary.wiley.com/doi/abs/10.1029/2019EF001170)
866 [2019EF001170](https://agupubs.onlinelibrary.wiley.com/doi/abs/10.1029/2019EF001170) doi: <https://doi.org/10.1029/2019EF001170>
- 867 Trenberth, K. E., & Shea, D. J. (2005). Relationships between precipitation and
868 surface temperature. *Geophysical Research Letters*, *32*(14). Retrieved
869 from [https://agupubs.onlinelibrary.wiley.com/doi/abs/10.1029/](https://agupubs.onlinelibrary.wiley.com/doi/abs/10.1029/2005GL022760)
870 [2005GL022760](https://agupubs.onlinelibrary.wiley.com/doi/abs/10.1029/2005GL022760) doi: <https://doi.org/10.1029/2005GL022760>
- 871 UNFCCC. (2015). *Adoption of the paris agreement. report no.*

- 872 *fccc/cp/2015/l.9/rev.1*. Retrieved from [http://unfccc.int/resource/](http://unfccc.int/resource/docs/2015/cop21/eng/109r01.pdf)
 873 [docs/2015/cop21/eng/109r01.pdf](http://unfccc.int/resource/docs/2015/cop21/eng/109r01.pdf)
- 874 Vogel, M. M., Zscheischler, J., Wartenburger, R., Dee, D., & Seneviratne, S. I.
 875 (2019). Concurrent 2018 hot extremes across northern hemisphere due to
 876 human-induced climate change. *Earth's Future*, 7(7), 692-703. Retrieved
 877 from [https://agupubs.onlinelibrary.wiley.com/doi/abs/10.1029/](https://agupubs.onlinelibrary.wiley.com/doi/abs/10.1029/2019EF001189)
 878 [2019EF001189](https://doi.org/10.1029/2019EF001189) doi: <https://doi.org/10.1029/2019EF001189>
- 879 von Trentini, F., Leduc, M., & Ludwig, R. (2019). Assessing natural variability
 880 in RCM signals: comparison of a multi model EURO-CORDEX ensemble
 881 with a 50-member single model large ensemble. *Climate Dynamics*, 53, 1963-
 882 1979. Retrieved from <https://doi.org/10.1007/s00382-019-04755-8> doi:
 883 [10.1007/s00382-019-04755-8](https://doi.org/10.1007/s00382-019-04755-8)
- 884 Wang, R., Lü, G., Ning, L., Yuan, L., & Li, L. (2021). Likelihood of compound
 885 dry and hot extremes increased with stronger dependence during warm
 886 seasons. *Atmospheric Research*, 260, 105692. Retrieved from [https://](https://www.sciencedirect.com/science/article/pii/S0169809521002489)
 887 www.sciencedirect.com/science/article/pii/S0169809521002489 doi:
 888 <https://doi.org/10.1016/j.atmosres.2021.105692>
- 889 Zink, M., Samaniego, L., Kumar, R., Thober, S., Mai, J., Schäfer, D., & Marx, A.
 890 (2016). The german drought monitor. *Environmental Research Letters*, 11(7),
 891 074002. Retrieved from [https://dx.doi.org/10.1088/1748-9326/11/7/](https://dx.doi.org/10.1088/1748-9326/11/7/074002)
 892 [074002](https://dx.doi.org/10.1088/1748-9326/11/7/074002) doi: [10.1088/1748-9326/11/7/074002](https://dx.doi.org/10.1088/1748-9326/11/7/074002)
- 893 Zscheischler, J., & Fischer, E. M. (2020). The record-breaking compound hot and
 894 dry 2018 growing season in germany. *Weather and Climate Extremes*, 29,
 895 100270. Retrieved from [https://www.sciencedirect.com/science/article/](https://www.sciencedirect.com/science/article/pii/S2212094719302002)
 896 [pii/S2212094719302002](https://www.sciencedirect.com/science/article/pii/S2212094719302002) doi: <https://doi.org/10.1016/j.wace.2020.100270>
- 897 Zscheischler, J., Martius, O., Westra, S., Bevacqua, E., Raymond, C., Horton,
 898 R. M., ... Vignotto, E. (2020). A typology of compound weather and
 899 climate events. *Nature Reviews Earth & Environment*, 1, 333-347. Re-
 900 trieved from <https://doi.org/10.1038/s43017-020-0060-z> doi:
 901 [10.1038/s43017-020-0060-z](https://doi.org/10.1038/s43017-020-0060-z)
- 902 Zscheischler, J., Orth, R., & Seneviratne, S. I. (2015). A submonthly database
 903 for detecting changes in vegetation-atmosphere coupling. *Geophysical*
 904 *Research Letters*, 42(22), 9816-9824. Retrieved from [https://agupubs](https://agupubs.onlinelibrary.wiley.com/doi/abs/10.1002/2015GL066563)
 905 [.onlinelibrary.wiley.com/doi/abs/10.1002/2015GL066563](https://agupubs.onlinelibrary.wiley.com/doi/abs/10.1002/2015GL066563) doi:
 906 <https://doi.org/10.1002/2015GL066563>
- 907 Zscheischler, J., & Seneviratne, S. I. (2017). Dependence of drivers affects risks as-
 908 sociated with compound events. *Science Advances*, 3(6), e1700263. Retrieved
 909 from <https://www.science.org/doi/abs/10.1126/sciadv.1700263> doi: [10](https://www.science.org/doi/abs/10.1126/sciadv.1700263)
 910 [.1126/sciadv.1700263](https://www.science.org/doi/abs/10.1126/sciadv.1700263)

Supporting Information for “Future hotspots of compound dry and hot summers emerge in European agricultural areas”

Andrea Böhnisch¹, Elizaveta Felsche^{1,2}, Magdalena Mittermeier¹, Benjamin

Poschlod³, Ralf Ludwig¹

¹Department of Geography, Ludwig-Maximilians-Universität München, Munich, Germany

²Center for Digital Technology and Management, Munich, Germany

³Research Unit Sustainability and Climate Risk, Center for Earth System Research and Sustainability, Universität Hamburg,

Hamburg, Germany

Contents of this file

1. Figures S1 to S3

Supplementary Figures

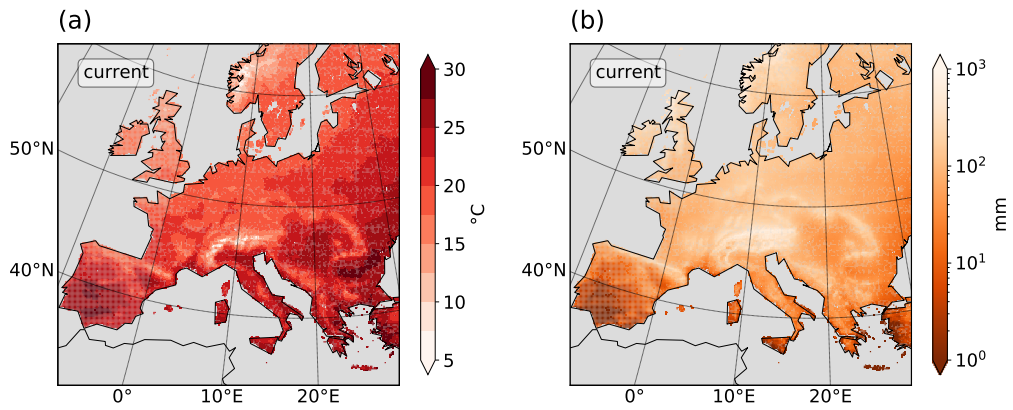


Figure S1. (a) 95th percentile of summer (June-July-August) temperatures across all CRCM5-LE members in Europe. (b) as (a) but for summer precipitation.

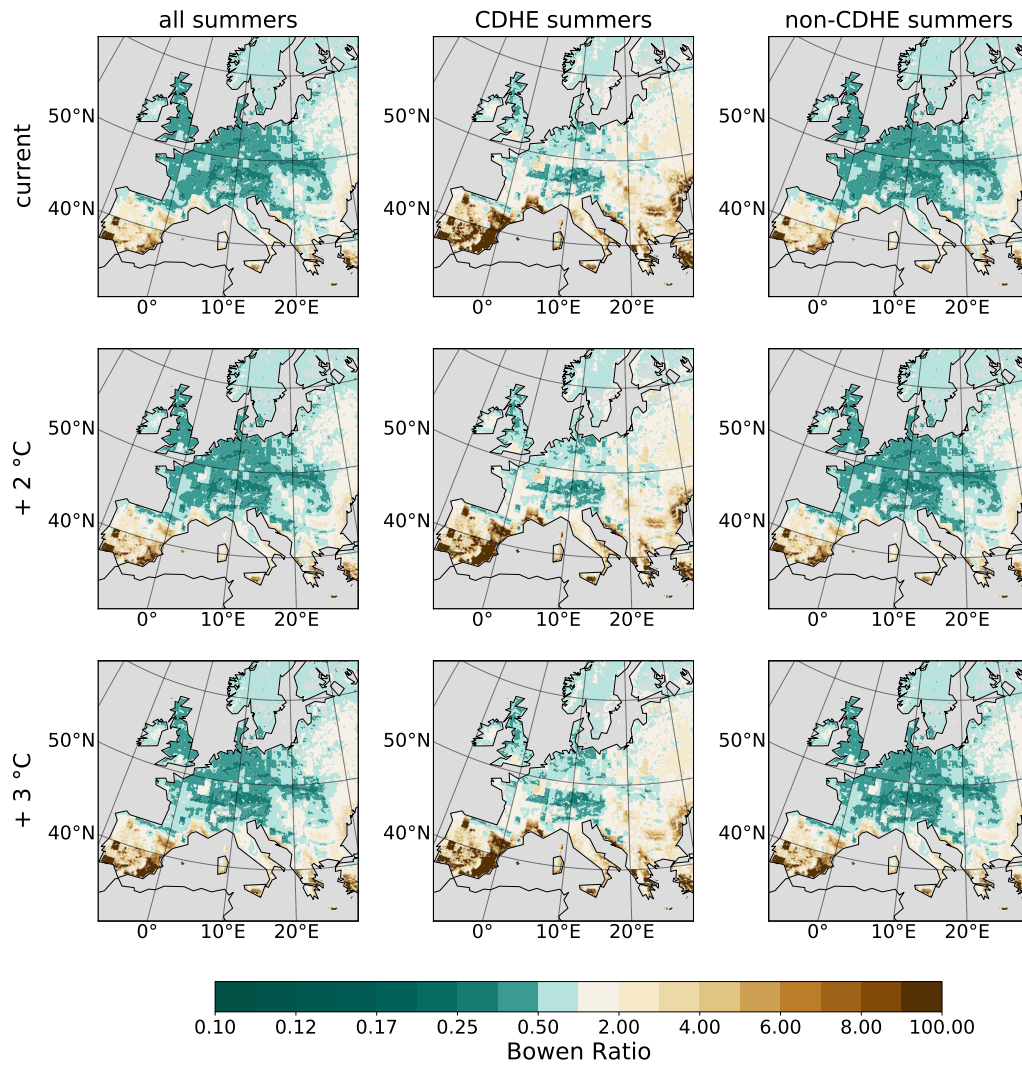


Figure S2. Bowen Ratio (BR) for all global warming levels (current, +2 °C, +3 °C; see main text). Columns show BR during all summers, CDHE-summers, and non-CDHE-summers.

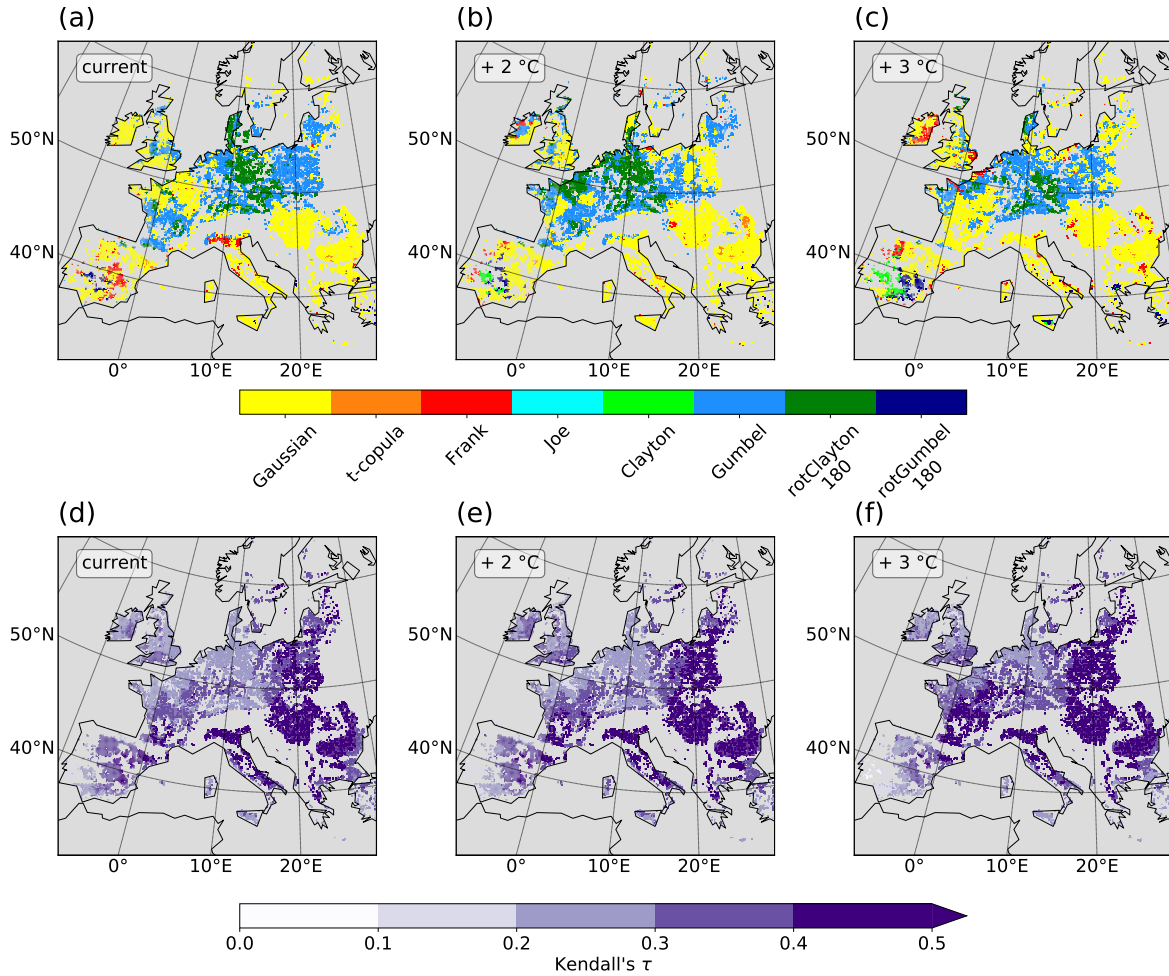


Figure S3. (a)–(c): Spatial distribution of fitted copula families for three global warming levels (current, +2 °C, +3 °C; see main text) in the CRCM5-LE. Yellow to red colors correspond to symmetric copula families, green to blue to asymmetric families, (d)–(f): theoretical Kendall's τ based on the copula family and parameter.